Wireless Personal Communications **5:** 223–258, 1997.

An Integrated Propagation-Mobility Interference Model for Microcell Network Coverage Prediction

BRENDAN C. JONES and DAVID J. SKELLERN
Electronics Department, School of Maths, Physics, Computing and Electronics, Macquarie University, NSW 2109 Australia. e-mail: brendan@mpce.mq.edu.au, and daves@mpce. mq.edu.au

Abstract. This paper presents a new interference model for microcellular networks which integrates radio propagation parameters and user terminal mobility. This model uses a parameter denoted the "interference to noise ratio" (INR) to obtain a simplified description of mobile link outage contours as a function of the location of the fixed and mobile radio ports. The INR is used to demonstrate that microcell networks are more interference limited than macrocell networks, and thus are more affected by user terminal mobility. Expressions are derived for the INR and user terminal cell radius distributions.

It is shown that in microcell systems a significant proportion of terminals may not be able to meet a contiguous coverage criterion, and that closer microcell spacing can reduce rather than improve the coverage quality. Examination of cochannel and adjacent channel reuse ratios in DCA microcell systems suggest that the closer frequency reuse is primarily responsible for these coverage effects. Monte Carlo simulations are used to test the analytical theory. These results may form the basis of a design methodology for microcell systems.

Key words: Interference modelling, microceus, radio coverage.

1. Introduction

The concept of cellular telephony is largely attributable to developments in radiotelephony at the Bell Telephone Laboratories from the late 1940s to the early 1970s [1, 2], and these developments led to the first commercial cellular telephone services being launched in the early 1980s [2, 3]. Since that time, the growth and popularity of mobile telecommunications has been extraordinary.

The capacity of cellular systems can be increased by splitting and sectorising existing cells, thereby reusing frequencies more often in a geographic area. In practice, however, there is a capacity limit as cells cannot be split indefinitely. The lower cell radius limit for most conventional cellular systems (herein referred to as "macrocells") is in the range of 1 to 1.5 km [4].

Microcell technologies are being developed to provide wireless communications to very large numbers of people at a much higher user density than is possible with macrocells [5]. Microcell architecture differs from macrocell architecture in three fundamental ways:

- The cells are typically less than 1 km in radius.
- The mobile terminals radiate at much lower power levels.
- All radio channels are available in every cell.

The wide scale deployment of an extensive, high grade, wireless telephone system will require engineering tools and techniques that allow rapid and accurate system design [4, 6]. The fundamental problem that needs to be addressed is modelling the end result of many users transmitting in a congested area [6].

As the number of deployed microcells increases, site-by-site engineering may become too time consuming and costly. Yet service quality targets, including cell coverage and call blocking and dropping probabilities, will need to be able to be predicted and met. This will require a design methodology that takes into account the competing requirements of minimising the number of cell sites, minimising the system roll-out time, and minimising the system design cost.

It has been claimed that "a well founded radio network planning methodology does not yet exist" [7] and certainly there does not yet appear to be a systematic design methodology for engineering a microcell network to a target service quality [4–13]. Consideration of service quality as part of the system design is an imperative because as the user base increases, people will no longer accept poor call quality simply because the service is "mobile" [13] but will demand a similar grade of service to that experienced in wireline services [4].

The applicability of macrocell design techniques to the microcell case is questionable. Firstly, macrocell systems use Fixed Channel Assignment (FCA) based upon an idealised, regular cell layout. This leads to a simple relationship between the "cluster size" C and the signal to interference (S/I) performance of a receiver at a cell boundary in the presence of cochannel interferers [14, 15]. However, no such simple relationship between cluster size and worst case S/I performance exists for microcells [16]. Microcell systems generally use Dynamic Channel Assignment (DCA) and the cochannel reuse statistics are difficult to predict.

Secondly, assumptions that only the cochannel interferers dominate in a macrocell system [10] may not be applicable in microcell systems [17] as it has been shown that adjacent channel interference (ACI) can affect the performance of heavily loaded cellular systems [18–20]. In practice, microcells often overlap and become irregular in shape [21], and the effects of ACI and further off-channel interference in microcells could be worse [17].

Thirdly, the close spacing of base stations in microcell systems (especially in multioperator environments) and closer frequency reuse have a very significant impact upon the percentage of service area that has a circuit quality better than some specified value [5, 22, 23]. Although the use of DCA and/or power control assists in controlling interference, these techniques can still fail under heavy traffic loads [23, 24]. The impact of spatial traffic variability and user terminal mobility also needs to be considered [21, 22, 25].

The combination of these factors may make it very difficult to engineer a microcell system so that reliable, contiguous radio coverage is achieved. Ubiquitous coverage may be impossible to achieve [26, 27].

This paper presents a microcell interference model that enables analysis of microcell coverage performance and could form the basis of a cell deployment methodology. The features of this model include:

- Uniform analysis of noise to interference limited environments.
- Incorporation of the cumulative interference effects of all users.
- Incorporation of terminal distribution models.

Both thermal noise and propagated interference are considered in the model because the transmission quality is strongly dependent upon these two factors [28]. The interference effects of all users are included in the model so as to avoid making assumptions about which interferers may dominate in the microcell environment.

Terminal distribution, hence mobility, is included in the model to avoid making assumptions about channel reuse distances. For example, Linnartz [29] assumed all interfering terminals in an FCA system were located at the reuse distance; Wang and Rappaport [17, 18] assumed

terminals were in the "worst case" location in each cell; and Chuang [30] assumed terminals were located at regular fixed points throughout the service area.

Other analyses, such as by Yao and Sheikh [31–34], Prasad and Kegel [35, 36] and Sowerby and Williamson [37] avoid explicit terminal distributions by instead assuming interferers have certain mean powers (the calculation of which is often left unstated), and that their power envelopes exhibit various statistics (e.g. Rice, Rayleigh, Nakagami, Suzuki) at the wanted receiver. Otherwise, numerical analysis via a Monte Carlo simulation is performed, whereupon terminals are randomly placed in some fashion, e.g. Button [38, 39], Driscoll [19].

Of these analyses, only Sowerby and Williamson [37] have attempted to analyse in spatial terms the quality of radio coverage achieved by mobile terminals, rather than just compute a blocking probability given the mean signal and interference powers at a receiver. Sowerby and Williamson, however, did not express their results in terms of the probability of terminals achieving an arbitrary cell radius, i.e. they did not calculate a cell radius distribution.

This paper demonstrates, in Section 2, the use of the microcell interference model in determining spatial outage contours in the presence of interferers and shows how cell coverage is affected by the degree of interference domination of wanted links, extending the work of Sowerby and Williamson [37] and Cook [40].

Monte Carlo simulations are presented in Section 3 to demonstrate the effects of user density and cell spacing on coverage in more complicated systems. In particular, the differences in the INR and cell radius distributions between microcell and macrocell systems are examined, and it is investigated as to whether microcell coverage can be improved by adjusting the cell spacing.

In Section 4 a mathematical analysis (under simplifying assumptions) is presented which illustrates how different terminal distribution models affect the INR and cell radius statistics. The results are compared with Monte Carlo simulations which do not make such simplifying assumptions. The cochannel and adjacent channel reuse statistics in DCA microcell systems are compared with macrocell systems, and their impact upon microcell performance is assessed. These results suggest that macrocell design principles cannot adequately predict microcell system performance and that the results obtained with the new model could form the basis of a microcell design methodology.

2. A Microcell Interference Model

2.1. General Network Model and Notation

Consider the microcell network in Figure 1, consisting of a fixed station F_0 and a mobile station M_{00} attempting to establish a radio link in the presence of n additional fixed stations $F_i\{1 \leqslant i \leqslant n\}$. Each fixed station communicates with additional mobile stations $M_{ij}\{1 \leqslant i \leqslant n, 1 \leqslant j \leqslant m_i\}$, where m_i is the total number of mobile stations communicating with fixed station F_i. The notation used for distances r between transmitters and receivers is as shown in Figure 1. Mobile terminal M_{ij} transmits to F_i at a power P_{Mij} on channel C_{Uij} (the *uplink*). Fixed station F_i transmits to mobile terminal M_{ij} at a power P_{Fij} on channel C_{Dij} (the *downlink*). The duplex channel C_{ij} may comprise a pair of time-division duplex (TDD) slots within the one radio carrier, a pair of time-division multiple access (TDMA) slots across a pair of radio carriers, or a pair of frequency division multiple access (FDMA) carriers.

Each transmitter radiates power not only into its intended channel but into other channels due to finite transmitter filter roll-off. This is called channel spill, and its magnitude depends

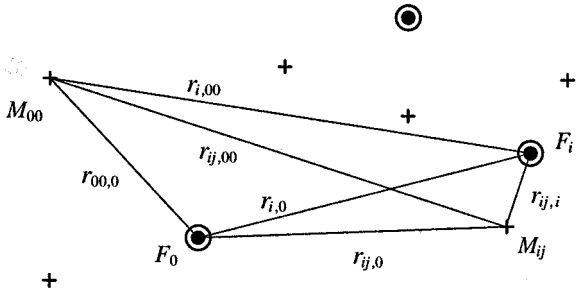

Figure 1. A general microcell model.

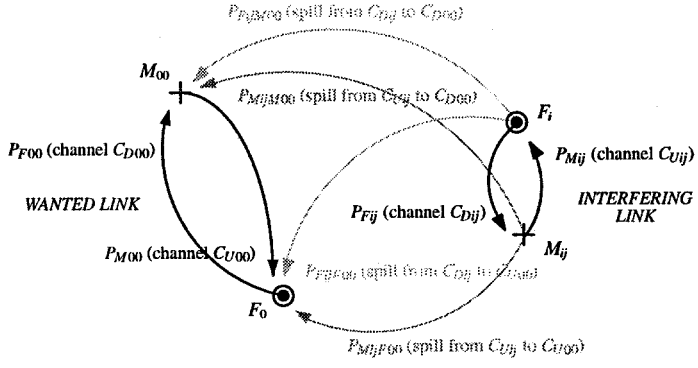

Figure 2. Model incorporating all transmitter to receiver interference components.

upon the radio modulation scheme, the multiple access method, the receiver filter shape, and the channel separation between the interfering and wanted channels.

Channel spills from transmitter to receiver are denoted P_{XijYkl} with X_{ij} indicating the transmitter and Y_{kl} the receiver. All four channel spill mechanisms are incorporated regardless of their magnitude at the source (i.e. all cochannel, immediately adjacent, and further channel spills are incorporated) because under high density user conditions, the cumulative interference from *all* users may become significant [17]. These interference components are illustrated in Figure 2.

Different propagation models are required for different environments. The simplest model is the single slope path loss model [41]:

$$P_r = \kappa P_t \left(\frac{d}{d_0}\right)^{-\gamma}, \quad d \geqslant d_0, \tag{1}$$

where P_r is the power received at a distance d (relative to the reference distance d_0) from a transmitter radiating at a power P_t. The parameter γ is the path loss exponent (in free space $\gamma = 2$) and κ is the free space path loss between the transmission antenna and the reference distance d_0:

$$\kappa = G_t G_r \left(\frac{\lambda}{4\pi d_0}\right)^2, \tag{2}$$

where G_t and G_r are the antenna gains of the transmitter and receiver respectively and λ is the wavelength of the transmission.

The single slope path loss model is used to describe the mean path loss in large area environments (i.e. macrocell environments) [42, 43]. In microcells, measurements have indicated that there is often a significant line of sight signal component. Propagation at close ranges therefore behaves more like the plane earth model and a dual slope path loss model is more appropriate [42–44]:

$$P_r = \begin{cases} \kappa P_t \left(\dfrac{d}{d_0}\right)^{-\gamma_1} & d_0 \leqslant d \leqslant b \\ \kappa P_t \left(\dfrac{b}{d_0}\right)^{-\gamma_1} \left(\dfrac{d}{b}\right)^{-\gamma_2} & b < d < \infty \end{cases}, \tag{3}$$

where b is the breakpoint distance, γ_1 is the path loss exponent before the breakpoint and γ_2 is the path loss exponent after the breakpoint. The breakpoint is related to the height above plane earth of the transmitter antenna h_t and receiver antenna h_r and is approximately given by [44]:

$$b = \frac{4h_t h_r}{\lambda}. \tag{4}$$

Equation (4) gives one theoretical expression for the breakpoint in the plane earth model, however the breakpoint is not well defined due to the oscillatory nature of the signal envelope in the plane earth model, and different definitions of where the breakpoint occurs gives slightly different expressions [45, 46].

Over a region of tens of wavelengths, a received signal will exhibit variation about the mean power predicted by the path loss models of (1) and (3). Measurements have consistently indicated these power variations exhibit lognormal statistics [41, 47]. This phenomenon is called lognormal shadowing and can be incorporated into either path loss model as a multiplicative factor to the path loss P_L:

$$P_r = P_L 10^{\zeta/10}, \tag{5}$$

where ζ is a normally distributed dB variable with zero mean ($\mu = 0$), and a standard deviation σ typically between 6 and 12 dB in macrocell systems [41] and 3 and 6 dB in microcell systems [43]. From (5) it can be seen that shadowing models both signal attenuation due to obstructions and signal amplification due to waveguiding effects.

2.2. Spatial Outage Analysis – One Interferer

At a receiver, a link will be considered successful if the signal to noise plus interference ratio $S/[N + I]$ is greater than or equal to the system protection ratio Z, otherwise an outage is deemed to occur. The region in which this threshold is maintained is the region in which radiocommunication is considered successful and is called the "cell". The extent of the cell is thus a function of the radio signal and interference statistics.

Examining Figure 1, assume M_{00} is communicating with F_{00} in the presence of a single interferer F_i which spills a power $P_{FiF00} = P_u$ into the wanted uplink and $P_{FiM00} = P_d$ into the wanted downlink. A spatial analysis of link outage in the presence of an interferer but in the absence of receiver noise was presented by Cook [40] using the single slope path loss model.

When the effect of receiver noise is incorporated (assuming that the same protection ratio applies to noise and interference), M_{00}'s uplink outage contour is a family of circles centred

on the fixed station F_0, but the downlink outage contour is a higher plane curve [48]. By introducing a parameter called the Interference to Noise Ratio (INR or η) the equations for both outage contours can be written in a simple form. The INR is the total interference power at a receiver divided by the receiver noise power. For a single interferer under the single slope path loss model, the uplink INR (i.e. the INR at the fixed station F_0) is given by [48]:

$$\eta_u = \frac{\kappa P_u r_{i,0}^{-\gamma}}{N}, \tag{6}$$

while the downlink INR (at the mobile terminal M_{00}) is given by:

$$\eta_d = \frac{\kappa P_d r_{i,00}^{-\gamma}}{N}. \tag{7}$$

Using this parameter, it can be shown that the equation for the uplink outage contour can be written [48]:

$$r_{00,0(u)}^{\gamma} = K_u r_{i,0}^{\gamma} \left[\frac{\eta_u}{\eta_u + 1}\right] = \psi \left[\frac{1}{\eta_u + 1}\right] \tag{8}$$

and the downlink outage contour equation can be written:

$$r_{00,0(d)}^{\gamma} = K_d r_{i,00}^{\gamma} \left[\frac{\eta_d}{\eta_d + 1}\right] = \psi \left[\frac{1}{\eta_d + 1}\right], \tag{9}$$

where $\psi = \kappa P_t / ZN$ and the parameter K is given by [40]:

$$K = \frac{P_t G_t G_r W_i L_s}{Z P_i W_t}, \tag{10}$$

where L_s is a system loss factor, P_i is the interference power, and W_i and W_t are the bandwidths of the interfering and wanted signals respectively. If these bandwidths are equal and G_t, G_r and L_s are unity, the expression simplifies to $K_d = P_t / ZP_d$ for the downlink and $K_u = P_t / ZP_u$ for the uplink. This parameter is a measure of the relative strength of the interferer.

By using the INR as a parameter, these equations provide a seamless description of the size and shape of the outage contours for all interference conditions from purely noise limited to purely interference limited. In the noise only case $(\eta = 0)$ the downlink and uplink outage contours are circles centred on F_0 of a radius determined by the receiver noise level. In the interference only case $(\eta \to \infty)$ the equations reduce to those in [40].

As the receiver $S/[N + I]$ threshold must be exceeded on both the uplink and downlink in order for the duplex link to be successful, the range of the mobile terminal M_{00} from F_0 in any direction is the minimum of r_u and r_d. Thus the range described by (8) represents the maximum possible range (i.e. cell radius) for M_{00} regardless of the downlink conditions.

2.3. Outage Contours – One Interferer

The downlink outage (9) can be rewritten in terms of η_u using the relationship $\eta_d = \eta_u (P_d / P_u)(r_{i,0} / r_{i,00})^{\gamma}$ [48] giving:

$$r_d^{\gamma} = r_{i,0}^{\gamma} [K_d - r_d^{\gamma} P_u r_{i,0}^{-\gamma} / P_d \eta_u]. \tag{11}$$

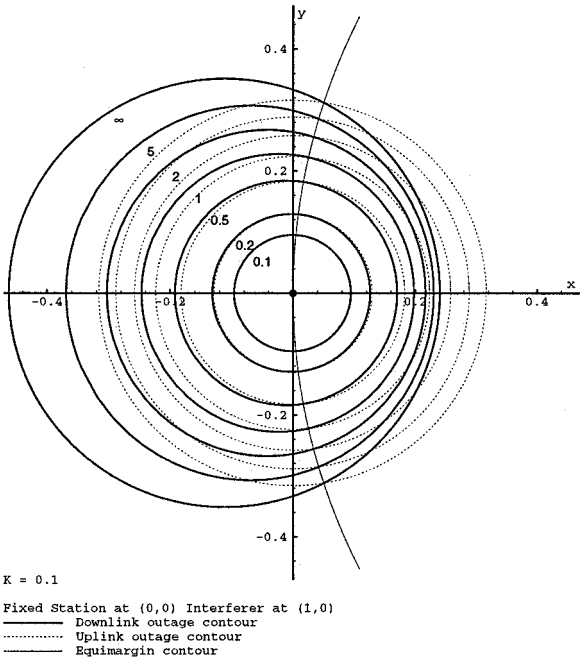

Figure 3. Outage contours for $K = 0.1$, $\gamma = 2$.

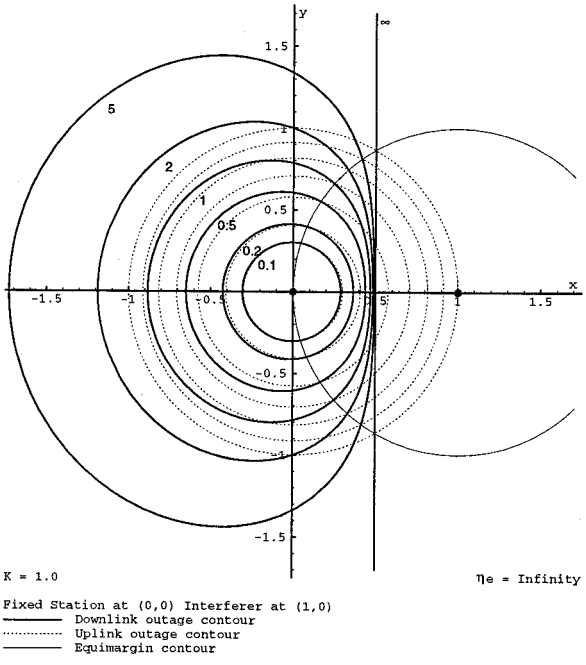

Figure 4. Outage contours for $K = 1.0$, $\gamma = 2$.

The uplink and downlink outage contours (as per (8) and (11) respectively) are plotted in Figures 3 to 6 for a range of η_u and for K of 0.1, 1.0, 10.0 and 100.0 and $\gamma = 2$.

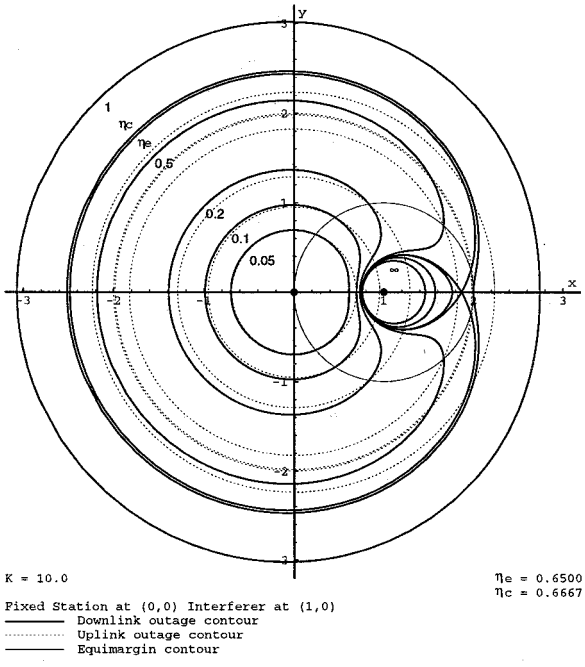

Figure 5. Outage contours for $K = 10.0$, $\gamma = 2$.

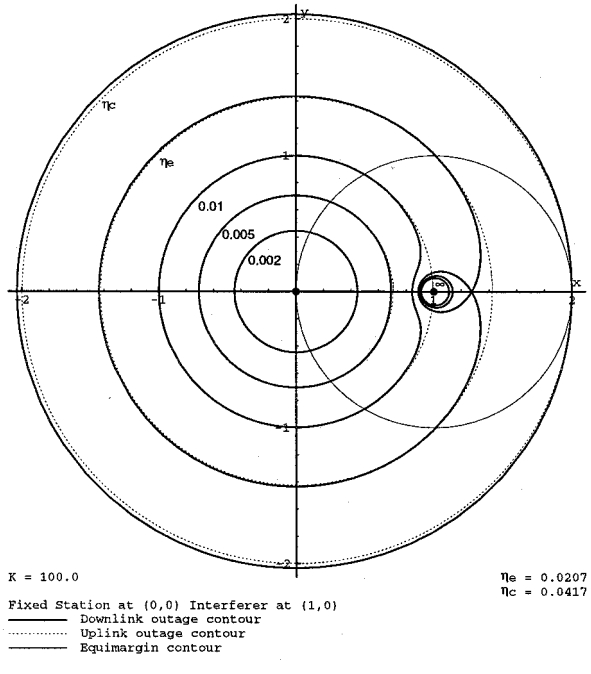

Figure 6. Outage contours for $K = 100.0$, $\gamma = 2$.

The value η_e in Figures 3 to 6 (that value of η_u at which the interferer is first enclosed by the downlink outage contour) can be shown to be given by [49]

$$\eta_e = [K_d^{1/(\gamma+1)} - 1]^{-(\gamma+1)} \tag{12}$$

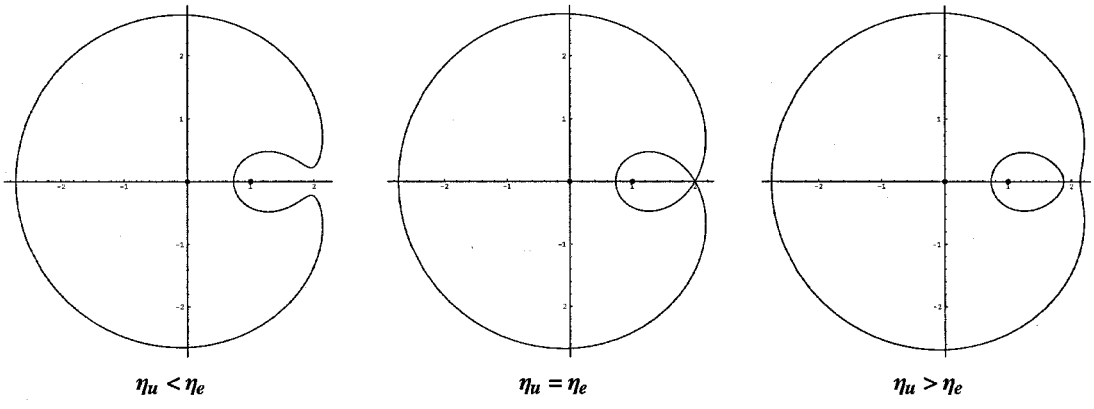

Figure 7. Downlink outage contour behaviour with $K > 1$ and the INR in the vicinity of η_e.

and if $K = K_u = K_d$ then η_c (that value of η_u at which the two outage contours intersect at a single point) can be shown to be given by:

$$\eta_c = \frac{2^\gamma}{K - 2^\gamma}, \tag{13}$$

$\eta_e > \eta_c$ for all K, except at $K = 2^{\gamma+1}$ whereupon $\eta_c = \eta_e = 1$. The equimargin contour (the contour where the uplink and downlink $S/[N + I]$ are the same) is a circle of radius $r_{i,0}$ centred on the interferer F_i.

Examining Figures 3 to 6 it can be seen that when the INR is small (i.e. $\eta_u < 0.1$) the uplink and downlink outage contours are approximately coincident circles, centred on the fixed station, at a radius determined by the receiver noise level (i.e. noise limited). When the INR is large (i.e. $\eta_u > 10.0$), the system is interference dominated and the downlink and uplink outage contours become quite different in size and shape.

Also Figures 3 to 6 show that when $K < 1$ communication on the downlink is limited to within the region $x \leqslant 0.5$, regardless of the INR. When $K > 1$ and the INR is in the vicinity of η_e the downlink outage contour exhibits the behaviour shown in Figure 7.

When $K > 1$ and $\eta_u < \eta_e$ the downlink outage contour bends around the interferer. When $\eta_u = \eta_e$ the downlink outage contour becomes limaçon-like, and just encloses the interferer (however, no limaçon can be made to match it exactly [50]). When $\eta_u > \eta_e$ the downlink outage contour has an inner and outer path, the inner path forming a "hole" in the communication region around the interferer. As $n_u \to \infty$ the outer outage path expands towards infinity, whereupon communication is possible on the downlink everywhere to the exterior of the inner outage path.

2.4. Spatial Outage Analysis – Two Interferers

Assume now that the wanted link M_{00} to F_0 operates in the presence of a fixed/mobile station pair F_i and M_{ij}. Assume that M_{00} and M_{ij}, as in Figure 1, move towards each other on the line joining F_0 and F_i, remaining equidistant from their respective fixed stations (i.e. $r_{00,0} = r_{ij,i}$), until each mobile terminal's link fails. The terminal range at outage then represents the worst-case proximity between these mobile terminals in neighbouring cells.

To simplify the notation for this situation, the separation between the fixed stations F_i and F_0 (i.e. $r_{i,0}$) will be denoted s. Using the parameter $\alpha (0 \leqslant \alpha \leqslant 1)$ the range of the mobile

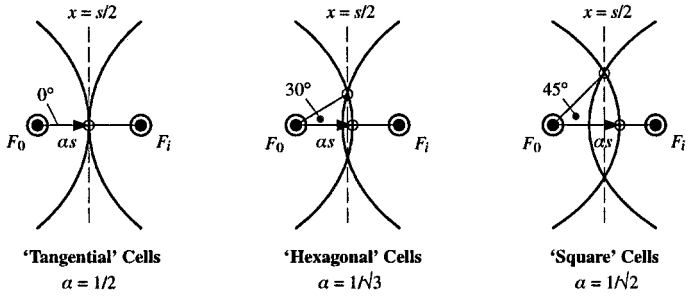

Figure 8. Three types of cell arrangements.

terminals can then be written as $r_{00,0} = r_{ij,i} = \alpha s$ and $r_{00,i} = r_{ij,0} = (1-\alpha)s$. Conditions can be attached to the relative outage range α of the mobile terminals in order to achieve certain cell coverage goals, such as tangential or overlapping coverage.

Three such goals are illustrated in Figure 8: "tangential" cell coverage, "hexagonal" cell coverage, and "square" cell coverage. Each provides progressively greater cell overlap. These goals represent a terminal range at outage of $s/2$, $s/\sqrt{3}$ and $s/\sqrt{2}$ respectively (i.e. $\alpha = \frac{1}{2}, 1/\sqrt{3}$ and $1/\sqrt{2}$ respectively).

If it is assumed that the channel spills are symmetrical between the mobile-fixed station pairs then $P_u = P_d = P_s$, the mutual spill power and $K_u = K_d = K$. It is also assumed that there is no fixed-to-fixed or mobile-to-mobile interference. Substituting αs for r_u and $(1-\alpha)s$ for $r_{ij,0}$ in the ψ form of (8) and solving for s gives [51]:

$$s = \frac{1}{\alpha}\left\{\frac{\kappa P_t}{N}\left(\frac{1}{Z} - \frac{P_s}{P_t}\left[\frac{\alpha}{1-\alpha}\right]^{\gamma}\right)\right\}^{1/\gamma}. \tag{14}$$

Equation (14) defines the worst-case fixed station separation s required to achieve cell overlap to the extent defined by α as a function of the relative mutual spill power P_s/P_t. Equation (14) may be plotted for an existing microcell technology such as CT2. Figure 9 shows the base station separation required as a function of the relative mutual spill power P_s/P_t (expressed in dBr) to maintain the three cell arrangements as shown in Figure 8 ($\gamma = 3.5$, $P_t = 10$ dBm, $Z = 14$ dB, $N = -111$ dBm).

Figure 9 shows that a specific cell coverage requirement demands smaller and smaller base station separations as the relative mutual spill power increases. The reduction in base station separation becomes extremely rapid near the "waterfall" part of each curve, and ultimately the target coverage criterion becomes impossible once the relative spill power exceeds a certain value.

As a microcell network becomes more highly interference limited, radio links in that network will operate more frequently near the waterfall part of the curves in Figure 9. Small amounts of additional interference will then greatly reduce the quality of cell coverage possible for those susceptible mobile links.

Thus a fixed coverage requirement imposes significant limits upon the accumulated interference allowable in a microcell system, and when those limits are exceeded, the proportion of mobile terminals that experience below target cell sizes will begin to grow. This could have severe ramifications upon the quality of cell coverage and the handoff reliability and thus the offered service quality.

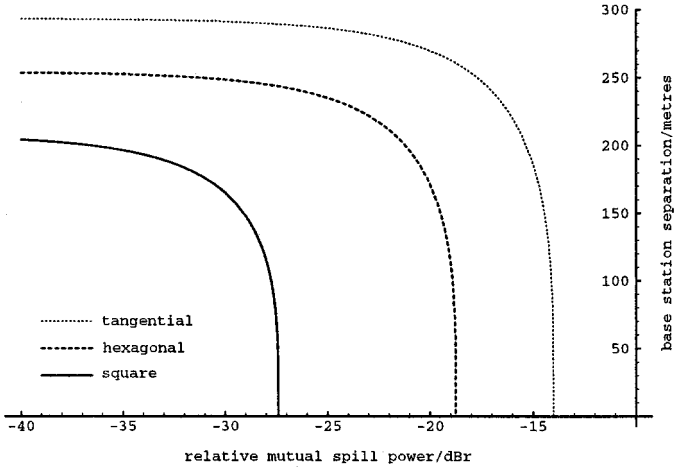

Figure 9. CT2 base station separation vs relative mutual spill power.

2.5. Spatial Outage Analysis – Arbitrary Numbers of Interferers

Consider an arbitrary mobile network with many transmitters, with notation as described in Figure 1. If it is assumed that all interference signals are uncorrelated with the wanted signal, the interference power I_{F00} received at fixed station F_0 in channel C_{U00} is the sum of all fixed-to-fixed station interference, all mobile-to-fixed station interference, plus receiver noise:

$$I_{F_{00}} = I_{FF_{00}} + I_{MF_{00}} + N. \tag{15}$$

The interference from fixed station F_i is the sum of all spills from transmissions to mobile terminals linked to that station. As these spills all emanate from F_i's antenna, the propagation range is $r_{i,0}$. The interference from mobile terminal M_{ij} is the spill from its transmission on channel C_{Uij} at the range $r_{ij,0}$. Using the single slope path loss propagation model, the total interference power received at F_0 in channel C_{U00} is given by:

$$I_{F_{00}} = \sum_{i=1}^{n}\left[\sum_{j=1}^{m_i}[\kappa_{ij}P_{F_{ij}}P_{F_{00}}]r_{i,0}^{-\gamma}\right] + \sum_{i=0}^{n}\left[\sum_{j=1}^{m_i}[\kappa_{ij}P_{M_{ij}F_{00}}r_{ij,0}^{-\gamma}]\right] + N. \tag{16}$$

The first summation subscript i begins at 1 as it is assumed that fixed stations (in this case, F_0) do not interfere with themselves (i.e. there is perfect isolation between all transmitters and receivers inside a fixed station).

The interference power I_{M00} received at the mobile terminal M_{00} in channel C_{D00} is the sum of all fixed to mobile terminal interference, all mobile to mobile terminal interference, plus receiver noise:

$$I_{M_{00}} = I_{FM_{00}} + I_{MM_{00}} + N. \tag{17}$$

Thus the total interference power received at M_{00} in channel C_{D00} is given by

$$I_{M_{00}} = \sum_{i=0}^{n}\left[\sum_{j=1}^{m_i}[\kappa_{ij}P_{F_{ij}}P_{M_{00}}]r_{i,00}^{-\gamma}\right] + \sum_{i=0}^{n}\left[\sum_{j=1}^{m_i}[\kappa_{ij}P_{M_{ij}M_{00}}r_{ij,00}^{-\gamma}]\right] + N. \tag{18}$$

Hence, the general forms of the INR become [49, 52]:

$$\eta_{u_{00}} = \frac{I_{FF_{00}} + I_{MF_{00}}}{N} = \frac{1}{N}\left\{\sum_{i=1}^{n}\left[\sum_{j=1}^{m_i}[\kappa_{ij}P_{F_{ij}F_{00}}]r_{i,0}^{-\gamma}\right] + \sum_{i=0}^{n}\left[\sum_{j=1}^{m_i}[\kappa_{ij}P_{M_{ij}F_{00}}r_{ij,0}^{-\gamma}]\right]\right\}, \quad (19)$$

$$\eta_{d_{00}} = \frac{I_{FM_{00}} + I_{MM_{00}}}{N} = \frac{1}{N}\left\{\sum_{i=0}^{n}\left[\sum_{j=1}^{m_i}[\kappa_{ij}P_{F_{ij}M_{00}}]r_{i,00}^{-\gamma}\right] + \sum_{i=0}^{n}\left[\sum_{j=1}^{m_i}[\kappa_{ij}P_{M_{ij}M_{00}}r_{ij,00}^{-\gamma}]\right]\right\}. \quad (20)$$

The outage contour expressions written in terms of the INR ((8) and (9)) still apply for the general uplink and downlink INR expressions [49].

The mobile to mobile or fixed station to fixed station interference can be very small. For example, if a TDD/TDMA system is assumed to be perfectly synchronised then all P_{FijF00} and P_{MijM00} terms will be zero. Further, the P_{MijF00} and P_{FijM00} terms will be zero between any two transmitters using different timeslots. If however, a TDD/TDMA system is not perfectly synchronised, then all interference terms could become significant.

In an FDMA system, the magnitude of the P_{FijF00} and P_{MijM00} terms depends upon the paired channel spill, i.e. how much RF radiation is spilled across the guard band used between the uplink/downlink channel pair. This spill value may be very small but it is usually not zero.

Equations (19) and (20) may be used to spatially determine where outage would occur if a mobile terminal (e.g. M_{00}) moved around the cellular service area, i.e. determine the extent of M_{00}'s cell. While (19) and (20) incorporate the impact of other interferers upon M_{00} as it moves within the service area, they do not consider M_{00}'s effect upon other receivers. If M_{00} moves close to another receiver M_{kl}, it may spill sufficient additional interference into M_{kl}'s receiver to cause an outage to M_{kl} but not to itself. Expressions for the regions in which this occurs were presented in [49].

3. Monte Carlo Simulation of Macrocell and Microcell Systems

3.1. Simulation Methodology

A computer program has been developed to model arbitrary cellular networks [49, 52]. The program can generate "snapshot" cell coverage plots or perform Monte Carlo simulations to estimate call blocking and dropout statistics, and INR and cell radius densities and distributions.

In each simulation, a random sequence of call attempts can be made from static mobile terminals randomly placed according to one of three distribution models. A mobile terminal's call attempt is deemed to fail if it doesn't meet the required $S/[N + I]$ on both the uplink and downlink. An initially successful mobile terminal can also drop out if the success of other terminals leads to an increase in interference, causing its $S/[N + I]$ to fall below threshold. In-cell channel reassignments and retries are permitted for DCA systems.

A "snapshot" cell plot comparison between a GSM system and a CT2 system was presented in [49] which suggested that microcells exhibit a larger degree of cell radius variation than

macrocells due to greater interference domination of wanted links. In [52] Monte Carlo simulations were performed to compare the INR and cell radius statistics of various macrocell and microcell technologies. These results showed microcell networks exhibiting larger INRs (around a factor of 100) and larger cell radius spread (around a factor of 10) than macrocell networks.

These simulations were based upon a single slope path loss propagation model and signal shadowing. The effects of using a dual slope model in the microcell case, and signal shadowing in all cases, are now examined.

3.2. Macrocell and Microcell INR and Cell Radius Statistics

The Monte Carlo simulation was loaded with the physical layer, call set up and channel allocation specifications for macrocell (AMPS and GSM) and microcell (CT2, DECT and PHS) technologies.

The number of *simultaneous* users per cell was adjusted in each system to achieve a comparable channel loading between the systems (10% of each cell's available channels). Cells were deployed in a regular hexagonal pattern of one central cluster of cells and one tier of surrounding clusters, at a spacing commensurate with high density deployment of the given technology. Table 1 summarises the simulation parameters used. A cluster size of unity means that all RF channels are available in every cell.

A single slope path loss model was used for macrocell environments and the dual slope model was used for microcell environments (as explained in Section 2.1). The path loss exponents and shadowing deviation values are representative values taken from measurements at appropriate frequencies and environments, reported by Marsan et al. [53], Seidel and Rappaport [54], Xia et al. [44, 43], and Feuerstein et al. [42]. The breakpoint in the dual slope path loss model assumed a lamp-post transmitter height of 6 m and a portable receiver at human ear height of 1.5 m.

In each simulation, approximately 10000 static call attempts were made. For DECT, CT2 and PHS, DCA was implemented in accordance with their specifications. Table 2 summarises the call failure statistics, including the rate of blocked and dropped calls. The average uplink INR (η_u) and standard deviation are also given for the *successful* terminals on a dB basis.

Finally, cell radius percentiles from the cell radius CDF are listed. For example, a "10% cell radius" of 100 m would indicate that 10% of *successful* terminals achieve a maximum cell radius of 100 m due to interference. Finally, the percentage of *successful* terminals which could maintain their link out to the target cell radius is given as "Contiguous Terminals (%)".

Table 2 shows the microcell systems modelled are significantly more interference limited (i.e. higher average η_u) than the macrocell systems by a factor of 30 to 40 dB. Under the dual slope path loss model, most microcell interferers lie within range of the path loss breakpoint. As the initial path loss is small, the interference effects are *worse* than that seen with the single slope, no shadowing model in [52]. Figure 10 plots the uplink INR (η_u) CDF on a lognormal scale for each technology, and the difference in the INR distributions between microcell and macrocell technologies is clear. The dashed lines represent the lognormal lines of best fit to each data.

Figure 11 shows the cell radius CDF computed from the INR CDF using (8) and the appropriate path loss model. The path loss breakpoints in the microcell model appears as a kink in the CDF traces for the microcell systems.

Table 1. Simulation parameters for five cellular technologies.

Parameter	AMPS	GSM	CT2	DECT	PHS
Cluster size	7	4	1	1	1
Target cell radius (m)	1500	1000	100	100	100
Simultaneous users per cell	12	25	4	12	30
Total number of cells	49	28	7	7	7
Total number of users	588	700	28	84	210
Portable Tx power (dBm)	29.0	29.0	10.0	24.0	19.0
Receiver noise floor (dBm)	−119	−110	−113	−101	−109
First path loss slope (γ_1)	3.0	3.0	1.5	1.3	1.3
Second path loss slope (γ_2)	—	—	6.0	8.0	8.0
Path loss breakpoint (m)	—	—	105	215	230
Shadowing deviation (dB)	10	10	4	6	6
Call setup S/I threshold (dB)	18	9	14	10	12

Table 2. Simulation results for five cellular technologies.

Parameter	AMPS	GSM	CT2	DECT	PHS
Call attempts	10584	10500	10024	10080	10080
Blocked calls (%)	34.2	17.7	0.19	4.84	8.06
Dropped calls (%)	9.5	7.0	0.03	1.17	4.36
Total call loss (%)	43.7	24.7	0.22	6.01	12.41
Average η_u (dB)	2.83	−2.04	33.97	32.83	43.82
10% cell rad (m)	879.6	845.7	113.7	218.4	64.3
5% cell rad (m)	699.6	683.5	97.3	140.7	45.4
2% cell rad (m)	552.7	523.0	65.6	76.6	30.8
1% cell rad (m)	484.5	438.0	53.5	53.1	24.3
Contiguous terminals (%)	44.5	84.4	94.7	97.0	80.7

The higher interference levels in the microcell systems lead to a greater spread of cell sizes, seen in Figure 11 and predicted by (8). In the macrocell systems, the cell radius at the tenth percentile is approximately 0.44 times that of the noise-limited cell radius. In the microcell systems, this factor is 0.26 for DECT, 0.18 for CT2 and 0.07 for PHS. Hence the

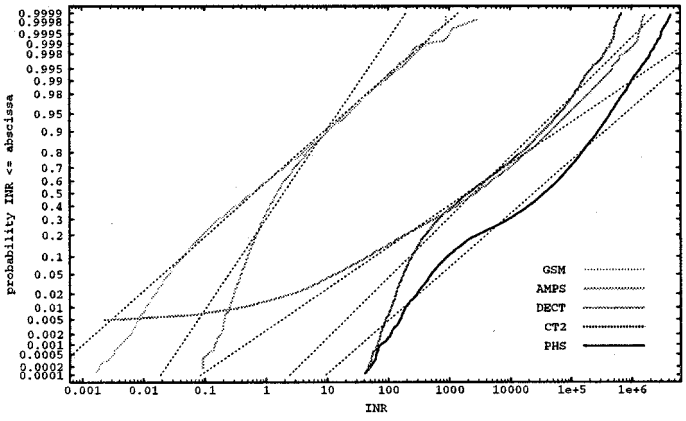

Figure 10. INR (η_F) CDFs for frive cellular technologies.

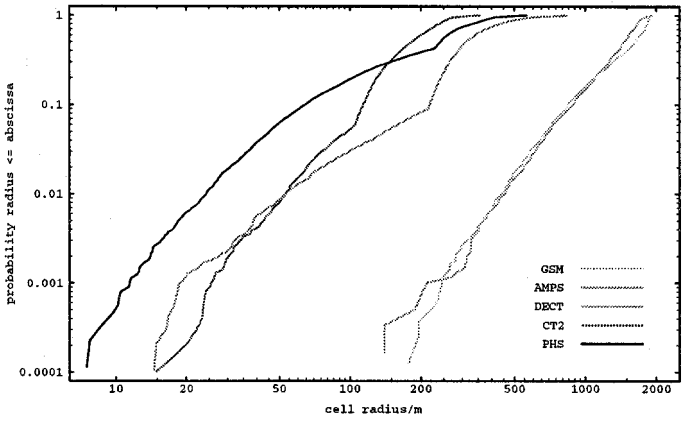

Figure 11. Cell radius CDFs for five cellular technologies.

spread of microcell radii is up to 6 times as great as that of macrocell radii. Compared at the first percentile cell radius, the microcell spread is even greater, by up to a factor of 9.

These results suggest that a significant proportion of mobile terminals in a microcell system may experience much smaller cells than the target radius specified by the fixed station separation, leading to significant coverage gaps and the potential for higher handoff failure rates.

3.3. Achieving Contiguous Coverage

The three most significant factors that may affect the probability of contiguous coverage in a microcell system are user density, cell spacing, and propagation model. To examine the effects of these parameters, a regular "hexagonal" network of 19 CT2 cells was simulated. Base stations were set $100\sqrt{3}$ m apart so that the mobile terminal range required for contiguous coverage was 100 m. The CT2 simulation parameters were as in Table 1 unless otherwise indicated.

Table 3. Simulation results for CT2 network.

Parameter	2 users/cell	4 users/cell	6 users/cell	8 users/cell
Blocked calls (%)	0.02	0.24	1.88	5.40
Dropped calls (%)	0.02	0.32	1.95	5.01
Total call loss (%)	0.04	0.56	3.84	10.42
Average η_u (dB)	30.37	36.84	40.05	41.81
Contiguous terminals (%)	97.2	93.3	89.7	86.0

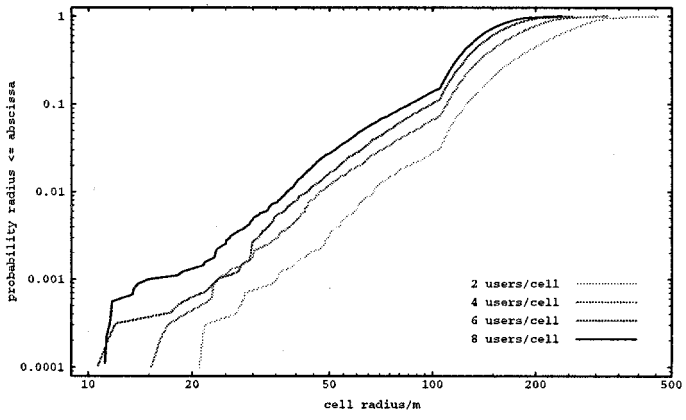

Figure 12. Cell radius CDF vs cell load.

Table 3 summarises the call failure, uplink INR (η_u), and contiguous coverage results as the traffic load was increased from 2 to 8 *simultaneous* users per CT2 cell. In each case, 10032 call attempts were made.

Table 3 indicates the average uplink INR increased with increasing traffic density (by approximately 6 dB for each doubling of the user load), and the proportion of blocked and dropped calls also increased, as expected. In addition, the proportion of successful terminals which could maintain their link to the target cell boundary decreased from 97% to 86%. The cell radius CDF, shown in Figure 12, shows how the spread of cell radii increases as user load per cell increases.

To explore a possible microcell design methodology, suppose a target is set that 95% of *successful* terminals should have contiguous coverage as determined by the fixed station layout. A microcell design strategy could involve reducing the fixed station separation until the contiguous coverage target is met. A number of 4 user/cell CT2 simulations were performed, with the cell spacing being reduced from $200\sqrt{3}$ m to $10\sqrt{3}$ m (i.e. the target cell radius was reduced from 200 m to 10 m). The proportion of contiguous terminals versus target cell radius is plotted in Figure 13.

It can be seen in Figure 13 that the proportion of contiguous terminals is not a simple function of the cell spacing. The highest proportion is achieved when the target cell radius is approximately equal to the path loss breakpoint (105 m in this simulation). This represents a compromise between achieving good signal power within a cell, but attenuating interferers outside the cell. Reducing the cell spacing increases the relative strength of nearby interferers, and the proportion of contiguous terminals begins to *decrease* with reduced separation. With

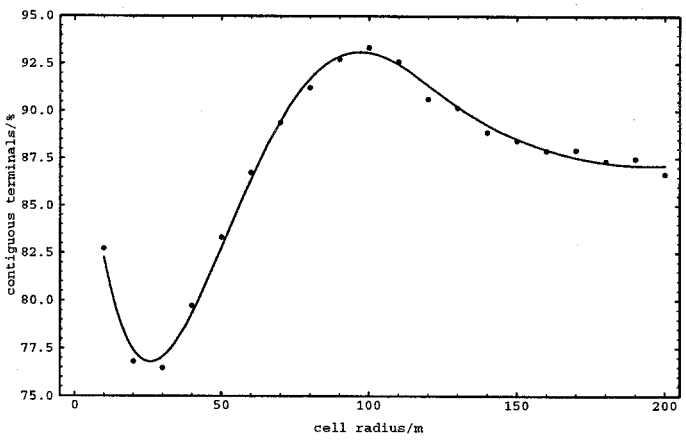

Figure 13. Proportion of successful mobile terminals with contiguous coverage vs cell radius.

a single slope path loss model and no signal shadowing, reducing the cell spacing results in a gradual improvement in the proportion of contiguous terminals, but an asymptotic limit is reached [55].

With very small cell spacing (below a cell radius of 30 m), the proportion of contiguous terminals begins to increase again. At these small separations, however, the call loss rate escalates rapidly (to over 40% below 20 m cell radius), greatly reducing total number of active interferers. This has the effect of increasing the proportion of contiguous terminals amongst those which were successful in establishing links.

Determining the "operating point" of a microcell system, i.e. meeting the desired service quality criteria in terms of the user load, terminal distribution and cell spacing may be very difficult. The critical parameters appear to be the closest approach of interferers (which is more ill-defined in DCA systems than FCA systems), the distribution of terminals, and the magnitude of adjacent channel spills. To progress, a theoretical understanding of these interference effects is needed.

4. Analysis of Interference and Cell Radius Statistics

4.1. Derivation of INR and Cell Radius Distributions

Equation (19) indicates the INR statistics are dependent upon the statistics of P_{FijF00} and P_{MijF00} (the spill powers), $r_{i,0}$ (a constant for each i) and $r_{ij,0}$ (the range of the interferer). With randomly placed terminals, $r_{ij,0}$ becomes a statistical quantity whose distribution may be derived for certain mobile terminal distributions. Then, with some simplifying assumptions, it is possible to derive expressions for the INR and cell radius statistics by following the process illustrated in Figure 14.

In Figure 14 the function f in the PDF domain represents a PDF transformation, and the function $\mathcal{F}$ in the CDF domain represents a CDF transformation.

Firstly, the PDF of the interfering terminal range $f_D(d)$ can be computed from the assumed terminal distribution. This incorporates mobility into the model. Next, the relationship between the interferer range and the INR $\eta = g(d..)$ enables the computation of the INR PDF $f_H(\eta)$. This incorporates the propagation and channel spill models. Finally, the relationship between

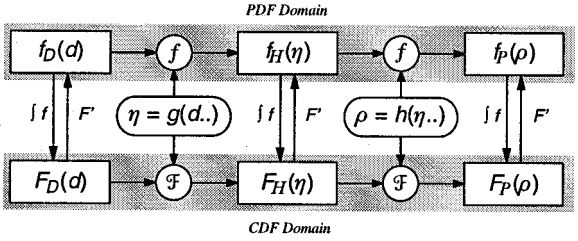

Figure 14. Process for deriving INR and cell radius statistics.

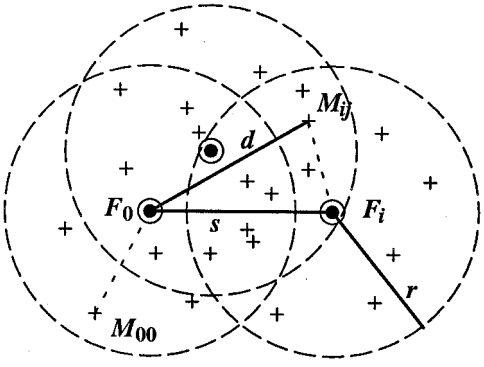

Figure 15. Non-roaming terminal microcell distribution model.

the INR and maximum cell radius $\rho = h(\eta..)$ enables the computation of cell radius PDF $f_P(\rho)$.

The CDFs may be obtained from the corresponding PDF by integration, or by transforming the previous CDF.

4.2. NON-ROAMING TERMINAL DISTRIBUTION MODEL

Consider a mobile terminal distribution where mobile terminals are randomly placed with a uniform distribution within the range r of a nominated server (Figure 15) and are permitted to access that server only. This model can demonstrate the effects of *near-far* interference.

Consider the simplest case of a two cell, two terminal system. In this case the interference model notation can be simplified as follows: $r_{i,0} = s, r_{ij,0} = d$, and if the two terminal transmissions are sufficiently orthogonal (e.g. DCA channel selections are well spaced), the channel spills $P_{FijF00} = P_{FF}$ and $P_{MijF00} = P_{MF}$ can be assumed to be constants [56]. This was denoted the "Equal Spill Theory" (EqS) [57].

Assuming the terminal distribution model of Figure 15, it can be shown that when $r \leqslant s$ the interferer range density function $f_D(d)$ is given by [56]:

$$f_D(d) = \frac{2d}{\pi r^2} \arccos\left[\frac{d^2 + s^2 - r^2}{2ds}\right] \quad s - r \leqslant d \leqslant s + r, \tag{21}$$

and when $r > s$ the interferer range density function is given by:

$$f_D(d) = \begin{cases} \dfrac{2d}{r^2} & 0 \leqslant d \leqslant r - s, \\ \dfrac{2d}{\pi r^2} \arccos\left[\dfrac{d^2 + s^2 - r^2}{2ds}\right] & r - s < d \leqslant s + r. \end{cases} \tag{22}$$

Initially the single slope path loss propagation model will be considered. For a pair of fixed stations, each communicating with one mobile station, η_u is found from (19), i.e.:

$$\eta_u = \frac{\kappa}{N}[P_{FF} s^{-\gamma} + P_{MF} d^{-\gamma}]. \tag{23}$$

The maximum cell radius achievable by the reference terminal M_{00} is denoted ρ and the random variable to which this value belongs P. The relationship between ρ (i.e. $r_{00,0}$) and η_u is given by (8).

Following the derivation procedure illustrated in Figure 14, the cell radius distribution function for the non-roaming terminal distribution model, when $r \leqslant s$, is given by [57]:

$$\begin{aligned} F_P(\rho) \;=\; 1 - \frac{1}{\pi r^2} \Bigg\{ & r^2 \arccos\left[\frac{\Lambda_\rho^2 - r^2 - s^2}{2rs}\right] - \Lambda_\rho^2 \arccos\left[\frac{\Lambda_\rho^2 - r^2 + s^2}{2s\Lambda_\rho}\right] \\ & + rs\sqrt{1 - \left(\frac{\Lambda_\rho^2 - r^2 - s^2}{2rs}\right)^2} \Bigg\}, \end{aligned} \tag{24}$$

where

$$\Lambda_\rho = \left\{ \frac{1}{P_{MF}} \left[\frac{N}{\kappa}(\psi \rho^{-\gamma} - 1) - P_{FF} s^{-\gamma} \right] \right\}^{-1/\gamma}. \tag{25}$$

When $r > s$ the distribution function becomes piecewise continuous. For $\rho > \rho_p$ the CDF of ρ is given by (24) where ρ_p is the breakpoint given by:

$$\rho_p = \left\{ \frac{\psi}{1 + \frac{\kappa}{N}[P_{FF} s^{-\gamma} + P_{MF}(r - s)^{-\gamma}]} \right\}^{1/\gamma} \tag{26}$$

and when $r > s$ and $\rho \leqslant \rho_p$ the CDF of ρ is given by:

$$F_P(\rho) = \frac{\Lambda_\rho^2}{r^2}. \tag{27}$$

This result is denoted the Equal-Spill Non-Roaming Theory (EqS–NR).

4.3. Constrained Non-Roaming Terminal Distribution Model

In this model, mobile terminals are distributed as in the previous model, except a constraint is applied that a terminal's nominated server must be the closest server. If this is not the case, that terminal is not admitted.

By restricting terminals to their closest server (usually done in practice on the basis of received signal strength indication – RSSI) the *near-far* problem of cell overlap is eliminated, and interference should be greatly reduced.

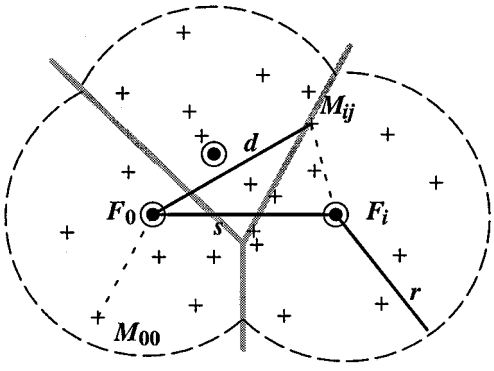

Figure 16. Roaming terminal microcell distribution model.

Consider again the two cell, two terminal case under the equal spill assumption and single slope path loss propagation model. If $r \leqslant s/2$ the cells are discrete and the distribution function $F_P(\rho)$ is given by (24). If $r > s/2$ the cells touch and the distribution function $F_P(\rho)$ becomes piecewise continuous about the point ρ_q which is given by [57]:

$$\rho_q = \left\{ \frac{\psi}{1 + \frac{\kappa}{N}[P_{FF} s^{-\gamma} + P_{MF} r^{-\gamma}]} \right\}^{1/\gamma}. \tag{28}$$

It can be shown that when $r > s/2$ and $\rho \leqslant \rho_q$ the distribution function $F_P(\rho)$ is given by [57]:

$$F_P(\rho) = \frac{\Lambda_\rho^2 \arccos\left(\frac{s}{2\Lambda_\rho}\right) - \frac{s}{4}\sqrt{4\Lambda_\rho^2 - s^2}}{r^2\left[\pi - \arccos\left(\frac{s}{2r}\right)\right] + \frac{s}{4}\sqrt{4r^2 - s^2}} \tag{29}$$

and when $r > s/2$ and $\rho > \rho_q$ the distribution function $F_P(\rho)$ is given by:

$$F_P(\rho) = \frac{\pi r^2 + \Lambda_\rho^2 \arccos\left[\dfrac{\Lambda_\rho^2 - r^2 + s^2}{2s\Lambda_\rho}\right] - r^2 \arccos\left[\dfrac{\Lambda_\rho^2 - r^2 - s^2}{2sr}\right]}{} \tag{30}$$

$$\frac{-rs\sqrt{1 - \left(\frac{\Lambda_\rho^2 - r^2 - s^2}{2rs}\right)^2} - r^2 \arccos\left(\frac{s}{2r}\right) + \frac{s}{4}\sqrt{4r^2 - s^2}}{r^2\left[\pi - \arccos\left(\frac{s}{2r}\right)\right] + \frac{s}{4}\sqrt{4r^2 - s^2}},$$

where Λ_ρ is given by (25). This result is denoted the Equal-Spill Constrained Non-Roaming Theory (EqS-CNR).

4.4. Roaming Terminal Distribution Model

Now consider a terminal distribution model with full inter-operator roaming. User terminals are placed randomly throughout the microcell *service area* with a uniform distribution and each mobile terminal chooses the "best" server on the basis of RSSI.

The grey lines in Figure 16 divide the service area into three regions where portable terminals will only access the server in that region. Clearly, this model can result in some servers handling more traffic than others.

Again consider the two cell, two terminal case under the equal spill assumption and single slope path loss propagation model. The set of possible server admissions $\mathcal{A}$ is divided into two mutually exclusive events:

- $\mathcal{S}$: The terminals choose the same server.
- $\mathcal{D}$: The terminals choose different servers.

The distribution function $F_P(\rho)$ can thus be computed for this model using the total probability theorem [58]:

$$F_P(\rho) = F_P(\rho|\mathcal{S})P(\mathcal{S}) + F_P(\rho|\mathcal{D})P(\mathcal{D}). \tag{31}$$

The distribution $F_P(\rho|\mathcal{D})$ is the Constrained Non-Roaming Terminal distribution given by (30). The distribution $F_P(\rho|\mathcal{S})$ is that resulting from same-cell interference. It can be shown that when $r > s/2$ and $\rho \leqslant \rho_s$ the distribution $F_P(\rho|\mathcal{S})$ is given by [57]:

$$F_P(\rho|\mathcal{S}) = \frac{\pi\zeta_\rho^2}{r^2\left[\pi - \arccos\left(\frac{s}{2r}\right)\right] + \frac{s}{4}\sqrt{4r^2 - s^2}} \tag{32}$$

and when $r > s/2$ and $\rho_s < \rho \leqslant \rho_r$:

$$F_P(\rho|\mathcal{S}) = \frac{\zeta_\rho^2\left[\pi - \arccos\left(\frac{s}{2\zeta_\rho}\right)\right] + \frac{s}{4}\sqrt{4\zeta_\rho^2 - s^2}}{r^2\left[\pi - \arccos\left(\frac{s}{2r}\right)\right] + \frac{s}{4}\sqrt{4r^2 - s^2}}, \tag{33}$$

where

$$\zeta_\rho = \left\{\frac{N}{\kappa P_{MF}}\left[\psi\rho^{-\gamma} - 1\right]\right\}^{-1/\gamma}, \tag{34}$$

$$\rho_r = \left\{\frac{\psi}{1 + \frac{\kappa}{N}[P_{MF}r^{-\gamma}]}\right\}^{1/\gamma}, \tag{35}$$

$$\rho_s = \left\{\frac{\psi}{1 + \frac{\kappa}{N}[2^\gamma P_{MF}s^{-\gamma}]}\right\}^{1/\gamma}. \tag{36}$$

Due to the symmetry of the two cell, two terminal system, clearly $P(\mathcal{S}) = P(\mathcal{D}) = 0.5$ thus $F_P(\rho) = 0.5[F_P(\rho|\mathcal{S}) + F_P(\rho|\mathcal{D})]$. The result is denoted the Equal-Spill Roaming Theory (EqS-R).

4.5. Comparison Between the Terminal Distribution Models – Theoretical

The three terminal distribution models may be compared by plotting their distribution functions for a specific case. Consider a two cell, two terminal CT2 system with the parameters as shown in Table 4. The CT2 system is assumed to be perfectly synchronised (i.e. all base stations transmit at exactly the same time, so there is no fixed-to-fixed station interference).

A constant channel spill P_{MF} of -49 dBc represents a situation where the DCA algorithm always maintains 3 or more RF channels between the two CT2 links (the EqS theory). In practice, some terminals may use closer channels (even under DCA) that spill greater amounts of power and thus create more interference. Note also the single slope path loss model

Table 4. CT2 simulation parameters.

Parameter	Value
γ	3.0
κ	−31.2 dB
N	−111.0 dBm
P_{FF}	0
P_{MF}	−49 dBc
r, s	100 m

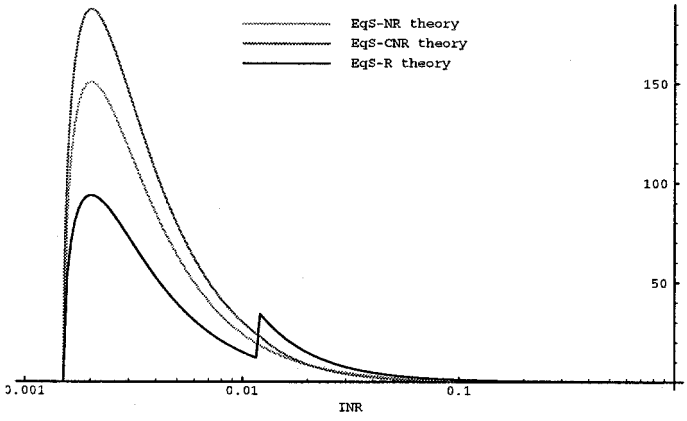

Figure 17. $f_H(\eta_F)$ for the three terminal distribution models.

is being used ($\gamma = 3.0$). Figures 17 to 19 show the resultant INR density $f_H(\eta_u)$, INR distribution $F_H(\eta_u)$, and cell radius distribution $F_P(\rho)$ functions respectively for the three terminal distribution models.

Figures 17 and 18 illustrate that all terminal distribution models have the same lower INR bound as a consequence of the cell layout geometry, but not the same upper bounds. All INR

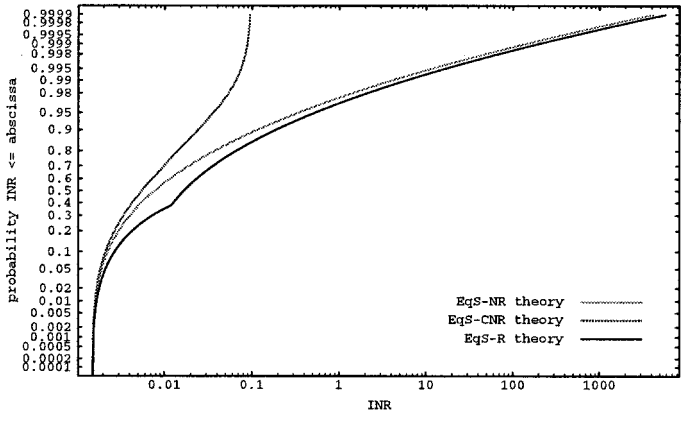

Figure 18. $F_H(\eta_F)$ for the three terminal distribution models.

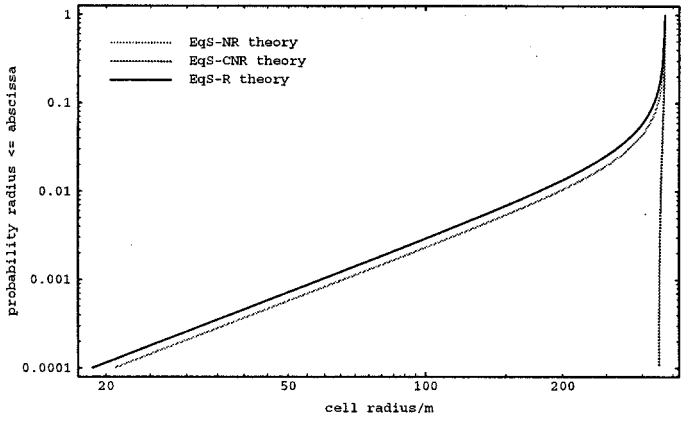

Figure 19. $F_P(\rho)$ for the three terminal distribution models.

densities exhibit a peak at low INR values, with a long tail that extends towards infinity if r approaches s. The EqS–R INR density function exhibits a step at the lowest INR value at which it is possible for the two terminals to choose the same server. This step appears as a kink in the INR distribution of Figure 18.

The EqS–CNR model leads to a very small spread of cell radii at around 330 m (Figure 19) as neither near-far nor same-cell interference is possible. The cell radii distributions, however, for the other two models are similar, suggesting that same-cell interference can be as deleterious to system performance as near-far interference. Also, even in the absence of cochannel and immediately adjacent channel interferers (the EqS simplification), interference from other users can lead to a significant reduction in cell radius.

4.6. Comparison Between the Terminal Distribution Models – Monte Carlo Simulation

The theoretical cell radius distribution results can be tested using the Monte Carlo microcell interference simulation program [49, 52] with mobile terminals placed in accordance with the terminal distribution models as described in Sections 4.2 to 4.4.

A two cell, two terminal CT2 network with simulation parameters as per Table 4 was implemented. Two simulations were then performed for each terminal distribution model, with cell radius statistics for the *successful* calls collected from 10000 random call attempts for each simulation condition.

The first simulation for each terminal distribution model applied the equal-spill assumption by constraining terminal transmissions to be at least 3 RF channels apart, giving a constant P_{MF} of -39 dBm. These simulations should agree closely with the EqS theory.

The second simulation allowed full DCA in accordance with the CT2 specification, hence P_{MF} varied in accordance with the actual channel allocations made at call set-up time (ETSI channel spills were used [59]). Simulations using full DCA and the ETSI spills are denoted "exact spill" (ExS) simulations and test the accuracy of the equal spill simplification.

Figure 20 shows the results for the Non-Roaming terminal distribution. The EqS–NR simulation follows the EqS–NR theory closely except for the last percentile of the distribution. This divergence is caused by the Monte Carlo simulation clearing calls which fail to meet the required $S/[N + I]$ while (24) is not conditional upon meeting the $S/[N + I]$ threshold.

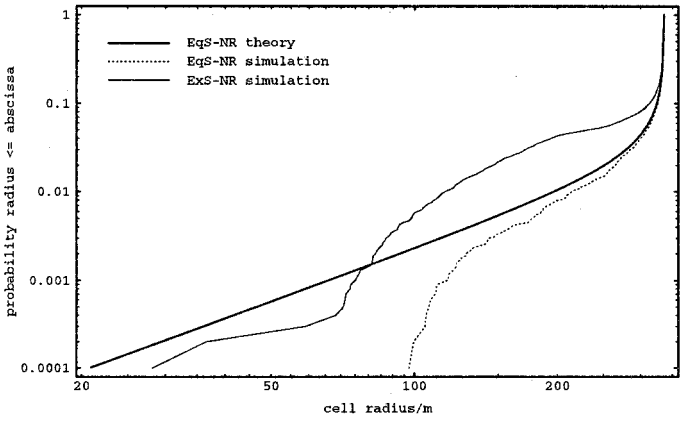

Figure 20. $F_P(\rho)$ for Non-Roaming terminal distribution.

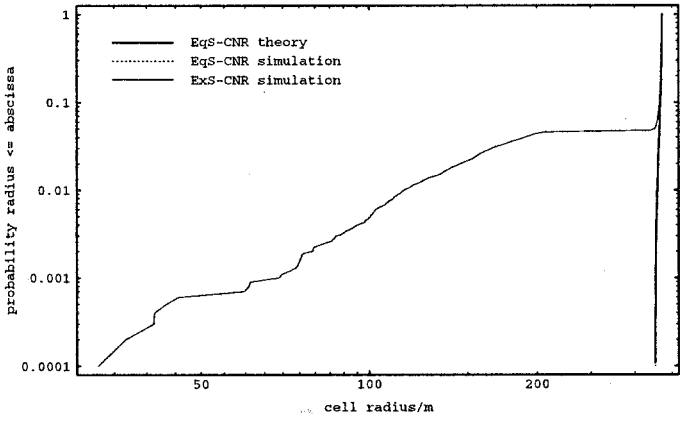

Figure 21. $F_P(\rho)$ for Constrained Non-Roaming terminal distribution.

Calls are more likely to be blocked or dropped if their INR is high or their maximum range is small. Hence the cell radius distribution for successful calls is skewed away from very small cell radii.

The ExS simulation compares reasonably well with the EqS theory save for the 1–5 percent region. With full DCA, it is possible for cochannel and immediately-adjacent channel interference to be generated. This increases interference and the probability of smaller cell radii until the $S/[N + I]$ constraint for a successful call comes into play. In all cases, it can be seen that near-far interference causes significant reductions in cell size.

The results for the Constrained Non-Roaming terminal distribution are shown in Figures 21 and 22 (Figure 22 expands the last part of Figure 21).

The agreement between the EqS–CNR simulation and theory is excellent, and the absence of near-far interference coupled with well spaced RF channels leads to a very small range of cell sizes as expected.

The ExS simulation, however, bears little resemblance to the EqS theory. This discrepancy is due to terminals in neighbouring cells choosing cochannels or adjacent channels under DCA. Such terminals can affect the system performance to the same degree as a close interferer choosing a well-spaced channel (ExS-NR result).

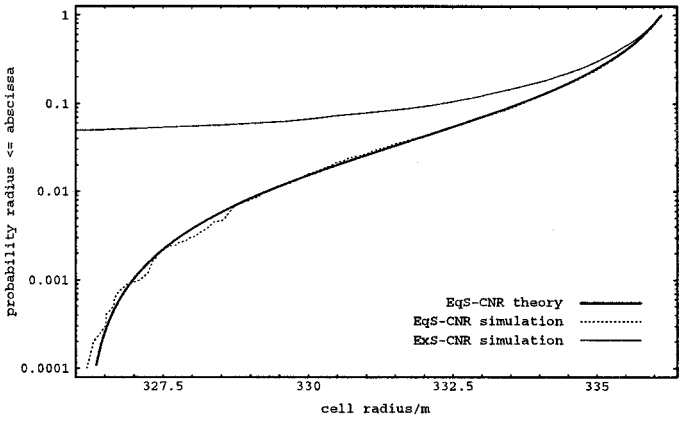

Figure 22. $F_P(\rho)$ – Expanded part of Figure 21.

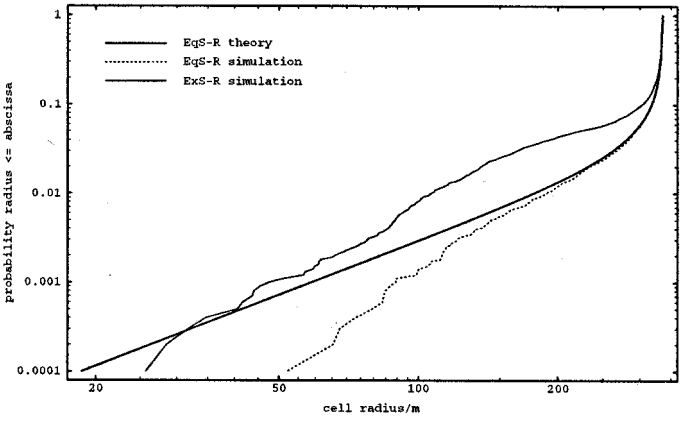

Figure 23. $F_P(\rho)$ for Roaming terminal distribution.

Further, the results of the roaming terminal distribution model (Figure 23) suggest that enabling roaming does not solve either problem. Roaming eliminates near-far interference, but the results in Figure 23 indicate that well spaced channels (EqS simulation) and DCA (ExS simulation) both cause same-cell interference, resulting in a significant reduction in cell radius for a significant proportion of terminals.

As the user density in a microcell system increases, such interference effects can only increase. Under high user density conditions it may not be sufficient to control microcell interference by using DCA and adopting strategies to combat the near/far problem.

In summary, the theoretical cell radius CDF is pessimistic in the region of interest (the last 10% to 1% of terminals) in comparison to the EqS simulation results, but is optimistic when the exact spills (ExS) are used.

4.7. NON-ROAMING TERMINAL DISTRIBUTION WITH DUAL SLOPE PATH LOSS MODEL

Returning to the non-roaming terminal distribution model of Section 4.2, the effect of a dual slope path loss model will now be considered. For a pair of fixed stations, each communicating with one mobile station, η_u may be written as:

$$\eta_u = \frac{\kappa}{N}[\Psi_F + \Psi_M], \tag{37}$$

where Ψ_F is the net fixed-to-fixed station channel spill and Ψ_M is the net mobile-to-fixed station channel spill under the prevailing propagation model. Under the dual slope path loss model and no shadowing, Ψ_F and Ψ_M are given by:

$$\Psi_F = \begin{cases} P_{FF} d_0^{\gamma_1} s^{-\gamma_1} & d_0 \leqslant s \leqslant b \\ P_{FF} d_0^{\gamma_1} b^{(\gamma_2-\gamma_1)} s^{-\gamma_2} & b < s < \infty \end{cases}, \tag{38}$$

$$\Psi_M = \begin{cases} P_{MF} d_0^{\gamma_1} d^{-\gamma_1} & d_0 \leqslant d \leqslant b \\ P_{MF} d_0^{\gamma_1} b^{(\gamma_2-\gamma_1)} d^{-\gamma_2} & b < d < \infty \end{cases}. \tag{39}$$

Introducing a constant φ_M defined as:

$$\varphi_M = \begin{cases} P_{MF} d_0^{\gamma_1} & d_0 \leqslant d \leqslant b \\ P_{MF} d_0^{\gamma_1} b^{(\gamma_2-\gamma_1)} & b < d < \infty \end{cases}. \tag{40}$$

Equation (37) may be rewritten as:

$$\eta_u = \begin{cases} \frac{\kappa}{N}[\Psi_F + \varphi_M d^{-\gamma_1}] & d_0 \leqslant d \leqslant b \\ \frac{\kappa}{N}[\Psi_F + \varphi_M d^{-\gamma_2}] & b < d < \infty \end{cases}. \tag{41}$$

The minimum INR η_{min} and maximum INR η_{max} are found by substituting $d = r + s$ and $d = s - r$ respectively into (41). One other value of importance is the INR at the path loss breakpoint η_b which is found by substituting $d = b$ into (41).

The maximum cell radius ρ achievable by the reference terminal is given by a two-slope path loss version of (8), i.e.:

$$\rho = \begin{cases} \left[\frac{\psi_b}{\eta_u + 1}\right]^{1/\gamma_1} & d_0 \leqslant \rho \leqslant b \\ \left[\frac{\psi_b}{\eta_u + 1}\right]^{1/\gamma_2} & b < \rho < \infty \end{cases}, \tag{42}$$

where

$$\psi_b = \begin{cases} \frac{\kappa P_t d_0^{\gamma_1}}{ZN} & d_0 \leqslant \rho \leqslant b \\ \frac{\kappa P_t d_0^{\gamma_1} b^{(\gamma_2-\gamma_1)}}{ZN} & b < \rho < \infty \end{cases}. \tag{43}$$

The minimum cell radius ρ_{min} maximum cell radius ρ_{max} and the cell radius at the INR breakpoint ρ_b are obtained by substituting η_{max}, η_{min} and η_b respectively for η_u in (42).

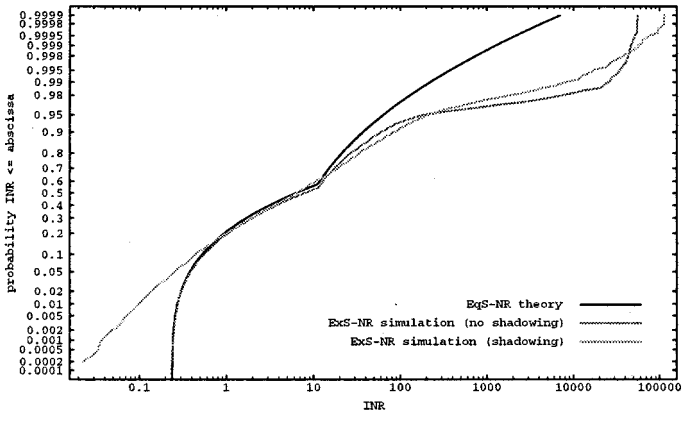

Figure 24. $F_H(\eta)$ for Non-Roaming terminal distribution – dual slope path loss.

The dual slope path loss model has two effects: it introduces a breakpoint into the interference distribution, and it effectively scales the impact of interferers outside of the path loss breakpoint. Hence the distribution functions presented in Sections 4.2 to 4.4 still apply provided the coefficients in the function are appropriately scaled.

For example, the cell radius distribution function for the non-roaming model is given by (24) when $r \leqslant s$. This function still applies under the dual slope model, except Λ_ρ is now scaled in accordance with the various breakpoints and path loss slopes:

$$\Lambda_\rho = \begin{cases} \left\{ \dfrac{\left[\frac{N}{\kappa}(\psi_b \rho^{-\gamma_1} - 1) - \Psi_F\right]}{P_{MF} d_0^{\gamma_1}} \right\}^{-1/\gamma_1} & \rho_{\min} \leqslant \rho \leqslant b \\ \left\{ \dfrac{\left[\frac{N}{\kappa}(\psi_b \rho^{-\gamma_2} - 1) - \Psi_F\right]}{P_{MF} d_0^{\gamma_1}} \right\}^{-1/\gamma_1} & b < \rho \leqslant \rho_b \\ \left\{ \dfrac{\left[\frac{N}{\kappa}(\psi_b \rho^{-\gamma_2} - 1) - \Psi_F\right]}{P_{MF} d_0^{\gamma_1} b^{(\gamma_2 - \gamma_1)}} \right\}^{-1/\gamma_2} & \rho_b < \rho \leqslant \rho_{\max} \end{cases} , \tag{44}$$

where ψ_b is given by (43) and Ψ_F is given by (38).

The two slope path loss model greatly changes the INR and cell radius distributions. The two cell, two terminal CT2 system as per Table 4 was simulated again, except with the two slope path loss model with $\gamma_1 = 1.5$, $\gamma_2 = 6.0$ and the path loss breakpoint $b = 105\,\text{m}$ (as per Table 1). Figure 24 shows the theoretical INR CDF compared with an exact spill Monte Carlo simulation (both with and without shadowing of $\sigma = 4\,\text{dB}$), and Figure 25 shows the theoretical cell radius CDF compared with an exact spill Monte Carlo simulation (again with and without shadowing).

The effect of the path loss breakpoint can be seen in the INR CDF at approximately $\eta_u = 10$ and in the cell radius CDF at the corresponding cell radius of approximately 400 m. A second breakpoint in the cell radius CDF occurs at $b = 105\,\text{m}$. This is visible in the simulated results, but is outside of the plot area for the theoretical curve.

The EqS theory performs slightly worse under the dual slope model compared with the single slope model. Reasonable accuracy is obtained to the 95th INR percentile and thus the

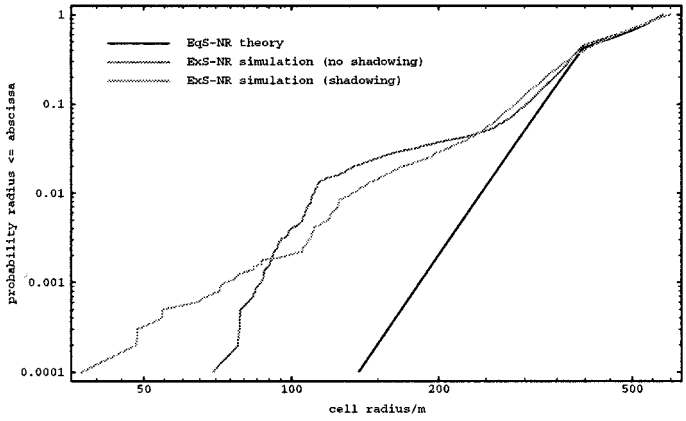

Figure 25. $F_P(\rho)$ for Non-Roaming terminal distribution – dual slope path loss.

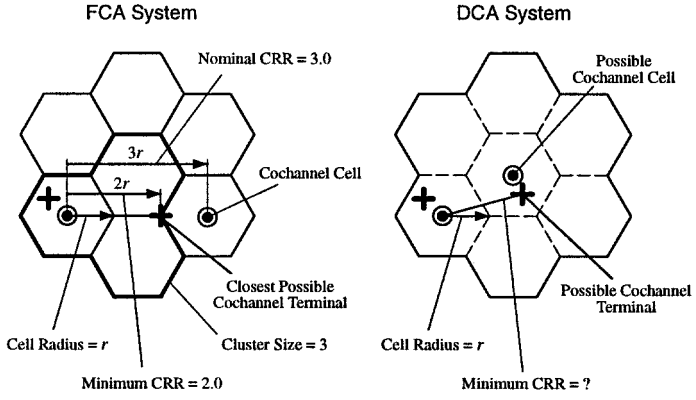

Figure 26. Cochannel reuse ratio in FCA vs DCA systems.

cell radius predictions down to the last 5% of terminals. After this point, however, its accuracy deteriorates rapidly. This is most likely due to the relatively stronger impact that cochannel and adjacent channel interferers have inside the path loss breakpoint under the two slope path loss model.

4.8. Channel Reuse Ratio Statistics

The results of the previous sections indicate that the probability of close interferers can dominate the extent to which cell radius reduction occurs for successful mobile terminals. In macrocell systems, the worst case $S/[N + I]$ performance is ideally constrained by FCA limiting the closest approach of cochannel and adjacent channel interferers. For example, in an FCA system with a cluster size of 3, the average cochannel reuse ratio (CRR) is approximately 3 and the minimum possible CRR is 2 due to the hard constraints designed into the system, as shown in Figure 26.

This design principle, however, breaks down in DCA microcell systems as every terminal has the capability of using any channel in any cell. In DCA systems there is not necessarily a guaranteed minimum cochannel reuse ratio (see Figure 26). The minimum CRR in microcell systems would be a complicated function of the terminal distribution, server access rules,

Table 5. Channel reuse ratio simulation results.

Parameter	GSM	CT2	DECT	PHS
Cells	21	21	21	21
Terminals	525	84	252	630
Call loss (%)	1.27	4.28	2.99	0.87
CCI events	2252	6881	11508	7885
Mean CRR	4.17	4.73	4.35	4.54
Min. CRR	2.04	1.33	1.20	1.25
ACI events	5375	18416	17268	19483
Mean ACRR	4.13	4.07	3.89	3.99
Min. ACRR	0.91	0.18	0.12	0.15

channel allocation algorithm, and previous channel selections, and cannot be adequately predicted using macrocell design principles [60].

To examine the CRR and ACRR (adjacent channel reuse ratio) performance of microcell systems, the Monte Carlo simulation program was used to simulate mobile networks with sufficient number of cells and terminals to generate a large number of cochannel and adjacent channel events.

A system of 21 cells arranged in a regular, hexagonal pattern was simulated for four cellular technologies (GSM, CT2, DECT and PHS). For the FCA system (GSM) the cluster size was set to 3 and the cells were spaced by $\sqrt{3}$ km, giving a target cell radius of 1 km. For the DCA microcell systems (CT2, DECT and PHS) the cells were spaced by $100\sqrt{3}$ m, giving a target cell radius of 100 m. The average number of terminals per cell was set to 10% of the total number of channels available in that cell for each technology simulated. The single slope path loss model was used in each simulation with $\gamma = 3.0$ so that any difference between FCA and DCA performance would be due to the channel access method rather than the propagation model.

In each simulation, terminals were randomly but uniformly placed within the 21 cell service area, and each terminal chose the "best" server at call setup time on the basis of RSSI. A total of 10000 static call attempts were made in each simulation, and whenever any pair of *successful* terminals were detected to be using the same or adjacent channel (and the same timeslot), the CRR or ACRR was calculated as appropriate. This ratio was calculated as the distance of the interfering terminal from the wanted terminal's fixed station divided by the target cell radius. The results of these simulations are summarised in Table 5 and the CRR and ACRR CDFs for each technology are plotted in Figures 27 and 28.

Table 5 shows that the minimum CRRs and ACRRs were much lower in the microcell systems than the macrocell system (GSM). Note that the average CRR/ACRR is largely determined by the system extent (number of cells) rather than any RF effect. Hence the CRR/ACRR distribution at *small* CRRs or ACRRs is critical, as the proportion of terminals successful with *small* CRRs or ACRRs will affect the quality of radio coverage.

Examining Figure 27, it can be seen that the microcell systems exhibit similar CRR CDFs, and that a significant proportion of cochannel terminals operated successfully at CRRs smaller than the smallest CRR possible for the GSM system modelled (2.0). From Figure 27, it can

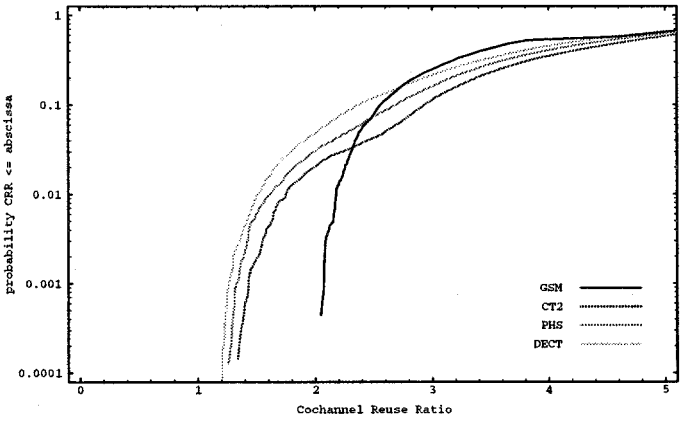

Figure 27. Cochannel reuse ratio CDF for four mobile technologies.

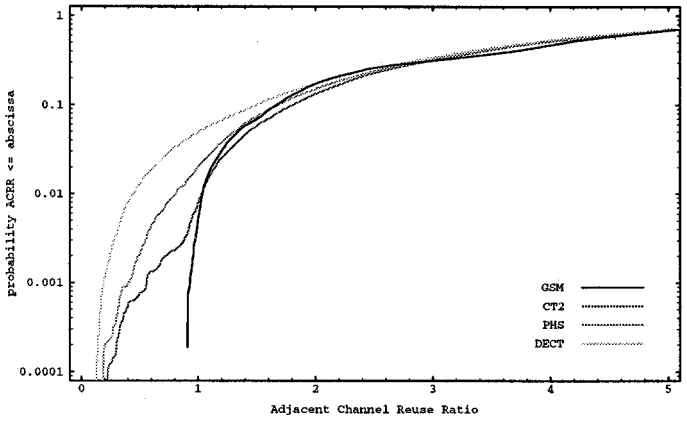

Figure 28. Adjacent channel reuse ratio CDF for four mobile technologies.

be seen that 1.9% of cochannel CT2 terminals, 3.0% of cochannel PHS terminals, and 4.5% of cochannel DECT terminals successfully operated at CRRs of less than 2.0.

Figure 27 also shows that RF blocking does eventually place a limit on the minimum CRR in a DCA system, however the lower limit is at different points for each microcell technology (from 1.20 for DECT to 1.33 for CT2) and cannot be predicted using macrocell (FCA) design principles.

Figure 28 shows that terminals in microcell systems also achieve significantly smaller ACRRs than in the macrocell system, with ACRRs as small as 0.12 being achieved whilst the minimum for GSM was 0.91 (FCA requires that all adjacent channel interferers lie outside the reference cell. With a hexagonal cell pattern the minimum possible ACRR is $\sqrt{3}/2 \approx 0.87$).

Such close channel reuse in microcell systems compromises coverage quality, as the earlier analytical and simulated results illustrated how close interferers greatly reduces the probability of a given terminal achieving a contiguous coverage range. Hence it would appear that the use of DCA in microcell systems is one of the factors contributing towards the fundamental performance differences observed between macrocell and microcell systems.

5. Conclusion

This paper has presented a new interference model for microcellular networks which can be used to model microcell coverage performance in terms of the broad system design parameters including propagation model, terminal distribution, cell spacing, user load, and channel spill.

Monte Carlo simulations and mathematical analysis have shown that DCA microcell systems are more highly interference limited, exhibit a greater cell radius variation, and have closer frequency reuse than FCA macrocell systems. These characteristics suggest that achieving reliable contiguous coverage in microcell systems will be difficult and will require a design approach different to that used in macrocell FCA systems.

In order to design a microcell system to meet given service quality targets, it has been proposed that the interference and cell radius statistics need to be derived or numerically estimated. It is proposed that the interference statistics obtained from the model provide a basis for determining the call blocking performance of the system, and that the cell radius statistics provide a basis for determining the cell spacing required in order to meet a coverage target for the offered user load. Developing these techniques could form the basis of a microcell design methodology.

Appendix – Notation and Acronym Glossary

Latin Notation

ACI	Adjacent Channel Interference
ACRR	Adjacent Channel Reuse Ratio
AMPS	Advanced Mobile Phone Service (US analog macrocell standard)
b	Breakpoint in the dual slope path loss model
C	Cluster size in an FCA system
C_{ij}	Duplex channel comprising an uplink channel C_{Uij} and a downlink channel C_{Dij}
C_{Dij}	Downlink channel ij (transmission from fixed station F_i to mobile terminal M_{ij})
C_{Uij}	Uplink channel ij (transmission from mobile terminal M_{ij} to fixed station F_i)
CDF	Cumulative Distribution Function
CRR	Cochannel Reuse Ratio
CT2	Cordless Telephone 2nd generation (digital microcell)
d	Distance variable
d_0	Reference distance in the distance-dependent path loss propagation model
DCA	Dynamic Channel Assignment
DECT	Digital European Cordless Telephone (digital microcell);
F_i	Fixed Station i
FCA	Fixed Channel Assignment
FDMA	Frequency Division Multiple Access
G_r, G_t	Receiver and Transmitter antenna gain
GSM	Groupe Special Mobile (also called Global System for Mobiles) (digital macrocell)
h_r, h_t	Receiver and Transmitter antenna heights
I_{Fij}	Total interference power received in channel C_{Uij} at fixed station F_i
I_{FFij}	Interference power received from all fixed stations in channel C_{Uij} at F_i
I_{FMij}	Interference power received from all fixed stations in channel C_{Dij} at M_{ij}
I_{Mij}	Total interference power received in channel C_{Dij} at mobile terminal M_{ij}
I_{MFij}	Interference power received from all mobile terminals in channel C_{Uij} at F_i
I_{MMij}	Interference power received from all mobile terminals in channel C_{Dij} at M_{ij}
INR	Interference to Noise Ratio (given the symbol η in equations)
K, K_d, K_u	Relative interferer strength. $K_d = P_t/ZP_d$ (downlink), $K_u = P_t/ZP_u$ (uplink)
M_{ij}	Mobile terminal j communicating with fixed station F_i
N	RMS Receiver Noise Power
P_d	Spill power into a wanted downlink (general)
P_{Fij}	Transmit power from fixed station F_i to mobile terminal M_{ij}
P_{FF}	Fixed station to fixed station spill power (general)

P_{FM}	Fixed station to mobile terminal spill power (general)
P_{Mij}	Transmit power from mobile terminal M_{ij} to fixed station F_i
P_r	Received power (general)
P_s	Channel Spill power (general)
P_t	Transmitted power (general)
P_u	Spill power into a wanted uplink (general)
P_{XijYkl}	Channel spill from X_{ij} to Y_{kl} (X_{ij} is the transmitter and Y_{kl} the receiver)
PDF	Probability Density Function
PHS	Personal Handy phone System (Japan) (digital microcell)
r	Cell radius (intended or target cell radius, usually a function of cell spacing)
r_d, r_u	Mobile terminal range at downlink and uplink failure (respectively)
$r_{i,k}$	Distance between fixed station F_i and fixed station F_k
$r_{ij,k}$	Distance between mobile terminal M_{ij} and fixed station F_k
$r_{ij,kl}$	Distance between mobile terminal M_{ij} and mobile terminal M_{kl}
RSSI	Received Signal Strength Indication
s	Fixed station separation (general)
S/I	Signal to Interference Ratio
$S/[N+I]$	Signal to Noise plus Interference Ratio
TDD	Time Division Duplex
TDMA	Time Division Multiple Access
Z	System interference protection ratio

Greek Notation

α	Outage range relative to fixed station separation
γ	Path loss exponent in a distance-dependent path loss propagation model
γ_1, γ_2	First and second path loss exponents in the dual slope path loss propagation model
η	Interference to Noise Ratio (general)
η_c	The uplink INR value at which the uplink and downlink outage contours intersect at a single point
η_e	The uplink INR value at which the interferer is first enclosed by the downlink outage contour
η_u	Uplink Interference to Noise Ratio (i.e. at a fixed station)
η_d	Downlink Interference to Noise Ratio (i.e. at a mobile terminal)
κ	The free space path loss from a transmit antenna to the reference distance d_0
λ	Wavelength of radio transmission
ρ	Maximum cell radius achievable by a mobile terminal
σ	Standard deviation of signal power in dB in the lognormal shadowing model
ζ	Normally distributed dB variable in the lognormal shadowing model
φ_M	Path loss constant in the dual slope path loss model
ψ	Technology dependent system constant $= \kappa P_t/ZN$
ψ_b	Technology dependent system constant in the dual slope path loss model
Ψ_F, Ψ_M	Net fixed to fixed station channel spill and mobile to fixed channel spill (respectively)

References

1. W.R. Young, “Advanced Mobile Phone Service: Introduction, Background and Objectives”, Bell System Technical Journal, Vol. 58 No. 1 pp. 1–14, Jan. 1979.
2. G. Calhoun, *Digital Cellular Radio*, Artech House, Massachusetts, USA, 1988.
3. J.D. Parsons and J.G. Gardiner, *Mobile Communications Systems*, Blackie and Sons, London, 1989.
4. J. Sarnecki, C. Vinodrai, A. Javed, P. O’Kelly and K. Dick, “Microcell Design Principles”, IEEE Communications Magazine, Vol. 31 No. 4 pp. 76–82, April 1993.
5. D.C. Cox, “Wireless Network Access for Personal Communications”, IEEE Communications Magazine, pp. 96-115, Dec. 1992.
6. T.S. Rappaport, “Wireless Personal Communications: Trends and Challenges”, IEEE Antennas and Propagation Magazine, Vol. 33 No. 5 pp. 19–29, Oct. 1991.
7. A. Gamst, “Remarks on Radio Network Planning”, Proceedings of the 37th IEEE Vehicular Technology Conference, p. 164, Tampa, 1–3 June 1987.

8. W.C.Y. Lee, "Smaller Cells for Greater Performance", IEEE Communications Magazine, Vol. 29 No. 11 pp. 19–23, Nov. 1991.
9. W.C.Y. Lee, "Quality and Capacity in Cellular", Electro International Conference Record, pp. 519–20, New York, USA, 16–18 Apr. 1991.
10. W.C.Y. Lee, "Spectrum Efficiency in Cellular", IEEE Transactions on Vehicular Technology, Vol. 38 No. 2 pp. 69–75, May 1989.
11. W.C.Y. Lee, "Estimate of Channel Capacity in Rayleigh Fading Environment", IEEE Transactions on Vehicular Technology, Vol. 39 No. 3 pp. 187–189, Aug. 1990.
12. J.G. Gardiner, "Second Generation Cordless (CT2) Telephony in the UK: Telepoint Services and the common air interface", Electronics and Communication Engineering Journal, pp. 71–78, April 1990.
13. I. Goetz, "Transmission Planning for Mobile Telecommunication Systems", 6th IEE International Conference on Mobile Radio and Personal Communications, pp. 126–130, Coventry, UK, 9–11 Dec. 1991.
14. V.H. MacDonald, "The Cellular Concept", Bell System Technical Journal, Vol. 58 No. 1 pp. 15–41, Jan. 1979.
15. W.C.Y. Lee, *Mobile Communications Design Fundamentals*, 2nd Ed., John Wiley and Sons, New York, 1993.
16. W.T. Webb, "Modulation Methods for PCNs", IEEE Communications Magazine, Vol. 30 No. 12 pp. 90-95, Dec 1992.
17. S.-W. Wang and S.S. Rappaport, "Signal to Interference Calculations for Corner Excited Cellular Communications Systems", IEEE Transactions on Communications, Vol. 39 No. 12 pp. 1886–1896, Dec. 1991.
18. S.-W. Wang and S.S Rappaport, "Signal to Interference Calculations for Balanced Channel Assignment Patterns in Cellular Communications Systems", IEEE Transactions on Communications, Vol. 37 No. 10 pp. 1077–1087, Oct. 1989.
19. J.P. Driscoll, "Relevance of Receiver Filter Perfrmance and Operating Range for CT2/CAI Telepoint Systems", Electronics Letters, Vol. 28 No. 13 pp. 1200–1201, 18 June 1992.
20. J.P. Driscoll, "Some Factors Which Affect the Traffic Capacity of a Small Telepoint Network", 5th IEE International Conference on Mobile Radio and Personal Communications, pp. 167–71, Coventry, UK, 11–14 Dec. 1989.
21. D. Everitt and D. Manfield, "Performance Analysis of Cellular Mobile Communications Systems with Dynamic Channel Assignment", IEEE Journal on Selected Areas of Communications, Vol. 7 No. 8 pp. 1172–1180, Oct. 1989.
22. A.O. Fapojuwo, A. McGirr and S. Kazeminejad, "A Simulation Study of Speech Traffic Capacity in Digital Cordless Telecommunications Systems", IEEE Transactions on Vehicular Technology, Vol. 41 No. 1 pp. 6–16, Feb. 1992.
23. P.A. Ramsdale, A.D. Hadden and P.S. Gaskell, "DCS1800 – The Standard for PCN", 6th IEE International Conference on Mobile Radio and Personal Communications, pp. 175–179, Coventry, UK, 9–11 Dec. 1991.
24. P.T.H. Chan, M. Palaniswami and D. Everitt, "Dynamic Channel Assignment for Cellular Mobile Radio System using Self-Organising Neural Networks", 6th Australian Teletraffic Research Seminar, pp. 89–95, Wollongong, Australia, 28–29 Nov. 1991.
25. S. Sato, K. Takeo, M. Nishino, Y. Amezawa and T. Suzuki, "A Performance Analysis on Nonuniform Traffic in Microcell Systems", IEEE International Conference on Communications (ICC 93), Vol. 3 pp. 1960–1964, Geneva, Switzerland, 23–26 May 1993.
26. S.T.S. Chia, "The Universal Mobile Telecommunication System", IEEE Communications Magazine, Vol. 30 No. 12 pp. 54–62, Dec. 1992.
27. S.T.S. Chia, "Providing Ubiquitous Cellular Coverage for a Dense Urban Environment", 44th Vehicular Technology Conference, pp. 1045–1049, Stockholm, Sweden, 8–10 June 1994.
28. A. Kegel, W. Hollemans and R. Prasad, "Performance Analysis of Interference and Noise Limited Cellular Land Mobile Radio", 41st IEEE Vehicular Technology Conference, pp. 817–821, St Louis, USA, 19–22 May 1991.
29. J.-P.M.G. Linnartz, "Exact Outage Analysis of the Outage Probability in Multiple-User Mobile Radio", IEEE Transactions on Communications, Vol. 40 No. 1, pp. 20–23, January 1992.
30. J.C.-I. Chuang, "Performance Limitations of TDD Wireless Personal Communications with Asynchronous Radio Ports", Electronics Letters, Vol. 28 No. 6, pp. 532–534, 12 March 1992.
31. Y.-D. Yao and A.U.H. Sheikh, "Outage Probability Analysis for Microcell Radio Systems with Cochannel Interferers in Rician/Rayleigh Fading Environment", Electronics Letters, Vol. 26 No. 13, pp. 864–866, 21 June 1990.
32. Y.-D. Yao and A.U.H. Sheikh, "Bit Error Probabilities of NCFSK and DPSK Signals in Microcellular Mobile Radio Systems", Electronics Letters, Vol. 28 No. 4, pp. 363–364, 13 February 1992.
33. Y.-D. Yao and A.U.H. Sheikh, "Performance Analyses of Microcellular Mobile Radio Systems with Shadowed Cochannel Interferers", Electronics Letters, Vol. 28 No. 9, pp. 839–841, 23 April 1992.

34. Y.-D. Yao and A.U.H. Sheikh, "Investigation into Cochannel Interference in Microcellular Mobile Radio Systems", IEEE Transactions on Vehicular Technology, Vol. 41 No. 2, pp. 114–123, May 1992.
35. R. Prasad, A. Kegel, J. Olsthoorn, "Spectrum Efficiency Analysis for Microcellular Mobile Radio Systems", Electronics Letters, Vol. 27 No. 5, pp. 423–425, 28 February 1991.
36. R. Prasad, A. Kegel and M.B. Loog, "Cochannel Interference Probability for Picocellular System with Multiple Rician Faded Interferers", Electronics Letters, Vol. 28 No. 24, pp. 2225–2226, 19 November 1992.
37. K.W. Sowerby and A.G. Williamson, "Outage Probabilities in Mobile Radio Systems Suffering Cochannel Interference", IEEE Journal on Selected Areas in Communications, pp. 516–522, Vol. 10 No. 3, April 1992.
38. J.E. Button, "Performance of CT2/CAI Systems in Small Cell Environments", Electronics Letters, Vol. 26 No. 18, pp. 1434–1436, 30 August 1990.
39. J.E. Button, "Asynchronous CT2/CAI Telepoint Separation Requirements", Electronics Letters, Vol. 27 No. 1, pp. 48–49, 3 January 1991.
40. C.E. Cook, "Modelling Interference Effects for Land Mobile and Air Mobile Communications", IEEE Transactions on Communications, Vol. 35 No. 2 pp. 151–165, Feb. 1987.
41. G.C. Hess, *Land-Mobile Radio System Engineering*, Artech House, Boston, 1993.
42. M.J. Feuerstein, K.L. Blackard, T.S. Rappaport, S.Y. Seidel and H.H. Xia, "Path Loss, Delay Spread and Outage Models as Functions of Antenna Height for Microcellular System Design", IEEE Transactions on Vehicular Technology, Vol. 43 No. 3 pp. 487–498, Aug. 1994.
43. H.H. Xia, H.L. Bertoni, L.R. Maciel, A. Lindsay-Stewart and R. Rowe, "Microcellular Propagation Characteristics for Personal Communications in Urban and Suburban Environments", IEEE Transactions on Vehicular Technology, Vol. 43 No. 3, pp. 743–751, Aug. 1994.
44. H.H. Xia, H.L. Bertoni, L.R. Maciel, A. Lindsay-Stewart and R. Rowe, "Radio Propagation Characteristics for Line-of-Sight and Personal Communications", IEEE Transactions on Antennas and Propagation, Vol. 41 No. 10 pp. 1439–1447, Oct. 1993.
45. V. Erceg, S. Ghassemzadeh, M. Taylor, D. Li and D.L. Schilling, "Urban/Suburban Out-of-sight Propagation Modelling", IEEE Communications Magazine, Vol. 30 No. 6 pp. 56–61, June 1992.
46. E. Green, "Radio Link Design for Microcellular Systems", British Telecom Technology Journal, Vol. 8 No. 1 pp. 85–96, Jan. 1990.
47. W.C. Jakes, *Microwave Mobile Communications*, IEEE Press, New York, 1974.
48. B.C. Jones and D.J. Skellern, "Interference Modelling and Outage Contours in Cellular and Microcellular Networks", 2nd MCRC International Conference on Mobile and Personal Communications Systems, pp. 149–158, Adelaide, Australia, 10–11 April 1995.
49. B.C. Jones and D.J. Skellern, "Spatial Outage Analysis in Cellular and Microcellular Networks", pp. 1–18, Wireless '95, Calgary, Canada, 10–12 July 1995.
50. E.H. Lockwood, *A Book Of Curves*, Cambridge University Press, England, 1967.
51. B.C. Jones and D.J. Skellern, "Designing the Ubiquitous Microcellular Network", Workshop on Applications of Radio Science (WARS '95), pp. I.8.1–I.8.4, Canberra, Australia, 25–27 June 1995.
52. B.C. Jones and D.J. Skellern, "Outage Contours and Cell Size Distributions in Cellular and Microcellular Networks", pp. 145–149, 45th IEEE Vehicular Technology Conference (VTC '95), Chicago, United States, 26–28 July 1995.
53. M.J. Marsan, G.C. Hess and S.S. Gilbert, "Shadowing variability in an Urban Land Mobile Environment at 900 MHz", Electronics Letters, Vol. 26 No. 10, pp. 646–648, 10 May 1990.
54. S.Y. Seidel, T.S. Rappaport, "Path Loss and Multipath Delay Statistics in Four European Cities for 900 MHz Cellular and Microcellular Communications", Electronics Letters, Vol. 26 No. 20 pp. 1713–1715, 27 Sept. 1990.
55. B.C. Jones and D.J. Skellern, "System Design for Contiguous Coverage in High Density Microcellular Networks", International Symposium on Signals, Systems and Electronics (ISSSE '95), pp. 263–266, San Francisco, United States, 25–27 October 1995.
56. B.C. Jones and D.J. Skellern, "Interference Distributions in Microcell Ensembles", 6th IEEE International Symposium on Personal, Indoor and Mobile Radio Communications (PIMRC '95), pp. 1372–1376, Toronto, Canada, 27–29 September 1995.
57. B.C. Jones and D.J. Skellern, "Influence of Terminal Distributions and Channel Spills on Microcell Coverage", IEEE 1995 Global Telecommunications Conference (Globecom '95), pp. 17–21, Singapore, 13–17 November 1995.
58. A. Papoulis, *Probability, Random Variables and Stochastic Processes*, 3rd Ed., McGraw Hill, New York, 1991.

59. European Telecommunications Standards Institute (ETSI), "Common Air Interface Specification between cordless telephone apparatus in the frequency band 864.1 MHz to 868.1 MHz", I-ETS 300–131, September 1991.
60. R. Saunders and L. Lopes, "Performance Comparison of Global and Distributed Dynamic Channel Allocation Algorithms", pp. 799-803, 44th IEEE Vehicular Technology Conference (VTC '94), Stockholm, Sweden, 8–10 June 1994.

Brendan Jones graduated in Electrical Engineering with First Class Honours from Newcastle University, Australia, in 1986, and was awarded second prize in the IEEE Region 10 Undergraduate Student Paper Competition that year. From 1987 to 1993 he worked in the Research and Development division of OTC Australia, one of Australia's international telecommunications carriers, and was involved in many research projects including microcellular modelling work for the OTC/Chevalier CT2 network in Hong Kong. From 1993 to 1996 he completed a PhD at Macquarie University in Sydney, Australia, investigating the modelling and analysis of interference in microcellular networks. In 1996 he was awarded first prize in both the Region 10 and Australia/New Zealand IEEE Postgraduate Student Paper Competitions. He now works for Optus Communications, Australia's second largest telecommunications company, as a technical specialist in mobile network planning. He has had over fifteen papers published.

David Skellern is the Professor of Electronics at Macquarie University. He holds the BSc (1972), BE (1974) and PhD (1985) degrees from the University of Sydney, Australia. From 1974 to 1983 he held various positions at the University of Sydney's Fleurs Radio Observatory.

His research since the mid 1980s, both in Australia and overseas, has involved collaboration with industry and research organisations on communications systems, circuit, and device design. At Macquarie University he has overseen major research programs in microelectronics, wireless communications networks and integrated services and is the author or co-author of over 30 journal articles and 80 conference papers in these research areas. Professor Skellern in the Chairman of the National Committee for Radio Science of the Australian Academy of Science, the Australian representative on Commission D (Electronic and Optical Devices and Applications) of the International Union for Radio Science (URSI), and a former Chairman of the Australian Telecommunications and Electronics Research Board.